UNIVERSITY OF OKLAHOMA

GRADUATE COLLEGE

MULTIFUNCTIONAL LIGHTWEIGHT POLYMER-BASED HYBRID COMPOSITES FOR PIEZOELECTRIC SENSING

A THESIS

SUBMITTED TO THE GRADUATE FACULTY

in partial fulfillment of the requirements for the

Degree of

MASTER OF SCIENCE

By ALEJANDRO X. SERRANO

Norman, Oklahoma

2026

Downloaded from SHAREOK. Persistent Handle URL: https://hdl.handle.net/11244/342521

MULTIFUNCTIONAL LIGHTWEIGHT POLYMER-BASED HYBRID COMPOSITES FOR PIEZOELECTRIC SENSING

A THESIS APPROVED FOR THE
SCHOOL OF AEROSPACE AND MECHANICAL ENGINEERING

BY THE COMMITTEE CONSISTING OF

Dr. Yijie Jiang, Chair

Dr. Hanping Ding

Dr. Jingyao Dai

©Copyright by ALEJANDRO X. SERRANO 2026
All Rights Reserved.

Table of Contents

Table of Figures vii
Table of Tables ix
Acknowledgements x
Abstract xii
Chapter 1: Introduction and Motivation 1
Chapter 2: Literature Review 5
2.1 Polymer Piezoelectric Systems 5
2.1.1 Piezoelectric Ceramics vs Polymer Systems 5
2.1.2 PVDF Crystalline Phases 7
2.2 Filler-Based Composite Behavior 9
2.2.1 Filler Loading Effects 10
2.2.2 Interfacial Interactions and Network Formation 12
2.3 Lightweight Filler Architectures 12
2.3.1 Hollow Microspheres and Density Reduction 13
2.3.2 Mechanical Compliance and Energy Absorption 14
2.4 DIW Processing and Network Effects 16
2.4.1 Rheology and Shear Alignment 16
Chapter 3: Materials and Experimental Methods 18
3.1 Materials 18
3.2 Preparation of PVDF-Coated Hollow Glass Microspheres 18
3.3 Composite Ink Preparation 19
3.4 Rheological Characterization of Inks 19
3.5 Direct Ink Writing (DIW) Fabrication 20
3.6 Mechanical and Electromechanical Testing 20
3.7 Thermal Characterization 21
3.7.1 Thermogravimetric Analysis (TGA) 21
3.7.2 Thermal Conductivity 22
3.7.3 Differential Scanning Calorimetry (DSC) 22
3.8 Dynamic Mechanical Analysis (DMA) 22

3.9 Dynamic Testing (Impact and Blast) 23
3.9.1 Drop Testing 23
3.9.2 Blast Testing 24
Chapter 4: Microstructure, Processing, and Physical Characteristics 25
4.1 Microstructural Characterization 25
4.1.2 Effect of Processing on Coating Uniformity 27
4.2 Rheological Behavior 30
4.3 Density and Structural Characteristics 32
Chapter 5: Mechanical, Functional, and Thermal Performance 35
5.1 Mechanical Behavior 35
5.1.1 Cyclic Stress-Strain Behavior 35
5.1.2 Specific Stress and Energy Absorption 36
5.1.3 Hyperelastic Modeling 38
5.1.4 Morphological Analysis After Deformation 39
5.2 Electromechanical Response 41
5.3 Dynamic Mechanical Analysis 43
5.4 Thermal Properties 45
5.4.1 Thermal Stability 45
5.4.2 Thermal Transport Properties 46
5.5 Dynamic Testing 47
Chapter 6: Computational Modeling and Potential Biomedical Applications 50
6.1 Introduction 50
6.2 Computational Modeling of Microstructure and Network Behavior 50
6.2.1 Modeling Approach 50
6.2.2 Network Formation and Percolation Behavior 52
6.2.3 Stress Distribution and Electromechanical Response 52
6.2.4 Discussion and Future Directions in Modeling 54
6.3 Bioinspired Electromechanical Sensing Application 55
6.3.1 Fabrication of Buckling Structure 55
6.3.2 Simulated Arterial Flow Setup 56
6.3.3 Electromechanical Response 57

6.3.4 Discussion and Application Outlook 59
6.4 Summary 60
Chapter 7: Conclusions 61
References 63

Table of Figures

Fig. 1: Piezoelectric performance comparison..... 7

Fig. 2: PVDF phases and transitions..... 9

Fig. 3: Filler percolation and response.....11

Fig. 4: DIW fabrication and structure..... 14

Fig. 5: Compressive behavior of composites..... 15

Fig. 6: Rheological behavior for DIW. 17

Fig. 7: PVDF-coated HGM characterization 27

Fig. 8: Coating uniformity and bridges..... 27

Fig. 9: Fluorine distribution analysis 28

Fig. 10: Nonuniform coating without ultrasonication..... 29

Fig. 11: Rheology and printability of inks 32

Fig. 12: Density versus filler loading..... 33

Fig. 13: Cyclic stress–strain hysteresis 36

Fig. 14: Specific stress and energy absorption..... 37

Fig. 15: Hyperelastic model fitting comparison 39

Fig. 16: Post-compression microstructural analysis 40

Fig. 17: Electromechanical and XRD characterization..... 42

Fig. 18: Viscoelastic behavior from DMA..... 44

Fig. 19: Thermal properties of composites 47

Fig. 20: Drop test piezoelectric response..... 48

Fig. 21: Blast-induced piezoelectric response 49

Fig. 22: Interparticle bridging and modeling..... 51

Fig. 23: FEA stress and displacement analysis 54

Fig. 24: DIW buckling structure fabrication 56

Fig. 25: Pulsatile flow voltage response 58

Table of Tables

Table 1: EDS composition of Sample 1 29

Table 2: EDS composition of Sample 2 30

Table 3: Hyperelastic model material parameters 39

Acknowledgements

I would like to start by thanking my advisor, Dr. Yijie Jiang, for his guidance and support throughout my graduate studies. His mentorship played a major role in my growth, not only as a researcher but also as a professional engineer. Through his feedback, expectations, and encouragement, I was able to develop a deeper understanding of the research process and improve the way I approach problems. I am truly grateful for the opportunities he provided and for the time he invested in helping me grow.

I would also like to acknowledge Dr. Wonbong Choi for his collaboration and contributions to this work. His insights and discussions played an important role in shaping parts of this research and broadening my perspective on its applications.

I would like to thank all my lab mates for their support throughout my research. Being part of the lab environment made this experience much more manageable and enjoyable. I would especially like to thank Maryam Tajik Hesaramiri and Rajan Rijal for their help along the way. Whether it was troubleshooting experiments, sharing ideas, or offering advice, their support made a big difference in this work.

I would like to thank Dr. Kuang Hua Chang for his continuous support and for the knowledge he shared with me, especially in developing my design and CAD skills. His guidance helped strengthen my engineering foundation and gave me confidence in my ability to approach design problems. I would also like to thank Dr. Preston Larson for his instruction and guidance in using the SEM, which was an important part of this research.

I am also grateful to my committee members, Dr. Jingyao Dai and Dr. Hanping Ding, for their time and for serving on my thesis committee. I appreciate their willingness to review my work and provide feedback that helped strengthen this thesis.

I would also like to acknowledge the financial and research support provided by the U.S. Department of Energy and Piezolabs Medical Inc. I would like to specifically thank the researchers and engineers at Piezolabs Medical Inc. for their valuable feedback and discussions throughout this project. Their input helped guide different aspects of this work and provided insight into real-world applications of the materials developed in this study.

Finally, I would like to thank my family. I could sit here and name every single one of them, because my whole family supported me throughout my academic journey, but I would like to especially mention Cynthia, Erica, and Veronica, my sisters who have been there for me throughout my entire life and every major moment along the way. I also want to thank my mother, Amparo, and my father, Jose. They tried their hardest to give my sisters and me everything we wanted growing up and continued to support us through everything. I would not be here without them.

Abstract

Lightweight and multifunctional polymer composites are widely used in aerospace, automotive, and biomedical applications. Piezoelectric materials enable the conversion between mechanical loads and electrical signals, which is critical for sensing applications; however, conventional piezoelectric materials are often limited by high density and brittleness. To address these limitations, polyvinylidene fluoride (PVDF)-coated hollow glass microspheres (HGMs) were used as a hybrid filler to introduce lightweight and electromechanical functionality into an elastomeric system. The HGMs were coated with PVDF using a high-power bladeless mixing process followed by ultrasonication to promote uniform surface coverage, then integrated into a polydimethylsiloxane (PDMS) matrix and processed via direct ink writing (DIW). The resulting composites exhibited a tunable reduction in density of up to two-fold, enhanced specific energy absorption, and improved voltage output under mechanical loading. Electromechanical testing demonstrated up to four-fold improvement in response compared to PDMS, with performance dependent on filler content and microstructural interactions. Thermal and rheological behavior further supported the tunability and printability of the system. A proof-of-concept buckling structure demonstrated measurable voltage generation under flow-induced deformation, highlighting the potential of these composites for soft sensing applications.

Chapter 1: Introduction and Motivation

The development of lightweight multifunctional materials has become increasingly important across a wide range of engineering applications, including aerospace structures, biomedical devices, wearable electronics, and soft robotic systems [1–5]. In many of these emerging technologies, materials are expected not only to provide mechanical support but also to enable additional functions such as sensing, actuation, or energy conversion. The integration of sensing capability directly into structural materials is particularly attractive because it enables the conversion of mechanical stimuli into electrical signals without requiring external sensing components [6,7]. This capability is essential for applications such as structural health monitoring, human motion detection, and impact sensing systems [8,9]. However, many conventional sensing technologies rely on rigid materials that are not well suited for integration with soft or deformable structures. While these materials can provide high sensitivity and stable electrical responses, their limited deformability often results in mechanical mismatch, stress concentrations, and reduced durability when embedded within flexible systems [10–12]. These limitations become especially problematic in applications that involve large mechanical strains, cyclic deformation, or conformal contact with biological tissues. As a result, significant research efforts have focused on developing material systems that combine mechanical compliance with reliable sensing functionality [13–15]. Piezoelectric materials provide a promising pathway for enabling this type of electromechanical response because they are capable of generating electrical charge when subjected to mechanical stress. This direct conversion between mechanical and electrical energy has been widely used in sensors, actuators, and energy harvesting devices. Traditionally, piezoelectric technologies have relied heavily on ceramic materials such as lead zirconate titanate (PZT) and barium titanate ($BaTiO_3$) due to their high piezoelectric coefficients and strong electromechanical coupling

[16,17]. Despite these advantages, ceramic piezoelectric materials are inherently brittle, relatively dense, and mechanically stiff, which limits their suitability for applications requiring flexibility or large deformation [18,19]. Additionally, concerns related to the toxicity of lead-based ceramics such as PZT, along with processing complexity, further restrict the widespread use of these materials [20]. In contrast, polymer-based piezoelectric materials offer a more mechanically compliant alternative that is compatible with flexible and deformable systems. Among these materials, polyvinylidene fluoride (PVDF) and its copolymers. such as poly(vinylidene fluoride–trifluoroethylene) (PVDF-TrFE), have received considerable attention because they exhibit piezoelectric behavior while maintaining the flexibility, toughness, and processability associated with polymer materials [21,22]. PVDF-based materials are capable of sustaining large mechanical strains without fracture and can be processed through a variety of manufacturing techniques, including solution processing, film fabrication, and additive manufacturing (AM) [22,23]. These characteristics make polymer-based piezoelectric materials attractive for developing soft sensing platforms and multifunctional composites. However, incorporating piezoelectric functionality into polymer composites introduces several design challenges [24,25]. A common approach involves dispersing piezoelectric particles or fibers within a polymer matrix to create a composite material capable of generating electrical signals during mechanical deformation. Although increasing the concentration of piezoelectric fillers can improve electrical response, high filler loadings often lead to undesirable effects such as increased material density, particle agglomeration, reduced mechanical compliance, and processing difficulties [26–28]. These issues highlight an important trade-off in conventional composite design, where improving electromechanical performance may compromise the mechanical properties required for flexible systems.

Consequently, there is growing interest in alternative composite architectures that enable piezoelectric functionality without relying solely on high concentrations of active filler materials. One promising strategy involves utilizing lightweight filler structures that can simultaneously influence mechanical behavior, density, and functional response within the composite [29,30]. Hollow microspheres have been widely used in polymer composites to reduce density and improve energy absorption characteristics while maintaining structural integrity [29–31]. By incorporating functional coatings or active materials onto these lightweight fillers, it becomes possible to create composite architectures in which the filler itself contributes to electromechanical functionality [32]. Such approaches allow the sensing capability of the composite to be distributed throughout the microstructure while preserving mechanical compliance and reducing overall material density.

In addition to materials design strategies, recent advances in manufacturing have created new opportunities for fabricating multifunctional polymer composites with controlled microstructures [33]. AM techniques such as direct ink writing (DIW) enable the fabrication of complex three-dimensional structures using viscoelastic inks that contain polymer matrices and functional fillers [34,35]. During extrusion-based printing processes, shear forces generated within the nozzle can influence the alignment of polymer chains and filler particles, which may further enhance the electromechanical response of the printed material [36]. As a result, AM methods not only provide a flexible fabrication route but also introduce additional mechanisms for tailoring composite microstructure and functionality [37].

Motivated by these considerations, this thesis explored a strategy by using hybrid fillers to functionalize lightweight polymer composites to enable integrated electromechanical sensing capabilities. The goal of this work is to develop composite material systems that combine reduced density, mechanical compliance, and piezoelectric functionality within a unified architecture. By

investigating the relationships between composite microstructure, processing methods, and material properties including electromechanical performance, this research aims to provide insights into the design of multifunctional lightweight materials suitable for applications in flexible sensing systems, impact detection technologies, and soft structural components.

Chapter 2: Literature Review

2.1 Polymer Piezoelectric Systems

Piezoelectric materials enable the direct conversion between mechanical stress and electrical charge, making them essential for sensing, actuation, and energy conversion applications [38,39]. Traditional piezoelectric devices have largely relied on ceramic materials because of their high electromechanical coupling and large piezoelectric coefficients [40–42]. However, the growing demand for flexible electronics, wearable technologies, and soft biomedical devices has motivated the exploration of alternative piezoelectric materials capable of operating reliably under large mechanical deformation [43,44]. Polymer-based piezoelectric material have therefore emerged as promising candidates due to their low density, mechanical flexibility, and compatibility with diverse fabrication processes [45,46]. Among these materials, PVDF has become one of the most widely studied piezoelectric polymers because of its stable electromechanical response and favorable mechanical properties [47,48]. Understanding the trade-offs between ceramic and polymer piezoelectric systems, as well as the structural mechanisms that enable polarization in PVDF, is essential for designing functional polymer-based piezoelectric composites.

2.1.1 Piezoelectric Ceramics vs Polymer Systems

Piezoelectric materials can generally be categorized into ceramic and polymer systems, each offering distinct advantages depending on the intended application [38,49]. Ceramic piezoelectric materials such as PZT and $BaTiO_3$ exhibit high piezoelectric coefficients and strong electromechanical coupling due to their highly ordered crystalline structures and large spontaneous polarization [9,50,51]. These properties make them highly effective in applications such as precision sensors, ultrasonic transducers, and actuators where strong electrical output is required

[52,53]. However, ceramic materials are inherently brittle and relatively dense, which limits their use in applications that require mechanical flexibility, large strain tolerance, or lightweight structures [16,54]. In contrast, polymer piezoelectric materials exhibit significantly greater mechanical compliance, lower density, and improved resistance to fracture under repeated deformation [22,55,56]. Although their intrinsic piezoelectric coefficients are typically lower than those of ceramic materials, polymers are well suited for flexible sensing applications where conformability, durability, and large strain capability are critical [57,58]. As illustrated in Figure 1a, ceramic materials occupy a region of high piezoelectric charge coefficients (d_{33}), while polymer-based materials such as PVDF exhibit lower d_{33} values but comparatively higher piezoelectric voltage coefficients (g_{33}), highlighting their effectiveness in voltage-based sensing applications [59]. Furthermore, Figure 1b illustrates the relationship between electromechanical performance and mechanical stiffness. Polymer-based materials occupy a low-stiffness regime with moderate energy harvesting figures of merit ($d_{33} \times g_{33}$), while ceramics and single crystals achieve higher performance at the expense of significantly increased stiffness . As a result, polymer piezoelectric materials have gained increasing attention for applications including wearable sensors, soft robotics, biomedical devices, and flexible electronics [3,4].

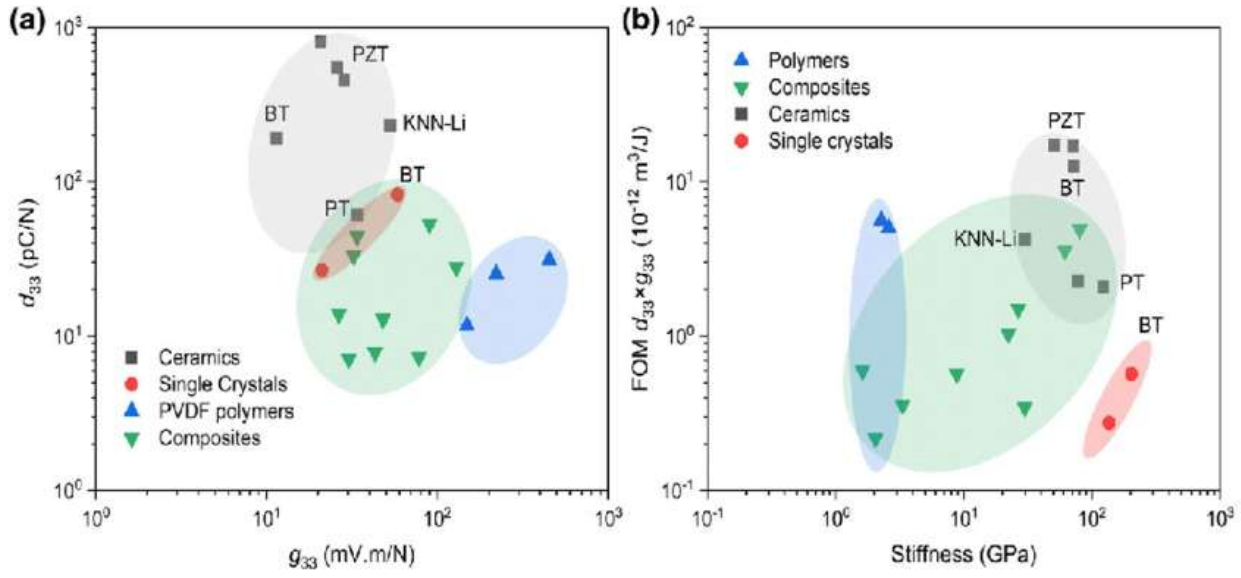


Fig. 1: Comparison of piezoelectric performance and mechanical stiffness for polymers, composites, ceramics, and single crystals [59]. (a) Piezoelectric coefficient, d_{33}versus piezoelectric voltage coefficient g_{33}. (b) Energy harvesting figure of merit ($d_{33} \times g_{33}$) versus stiffness.

2.1.2 PVDF Crystalline Phases

Among polymer-based piezoelectric materials, PVDF and its copolymers have attracted significant attention due to their strong molecular dipole moment and favorable mechanical behavior [22,60]. PVDF is a semicrystalline fluoropolymer that can crystallize into several polymorphic phases, including the α, β, and γ phases, each characterized by distinct molecular conformations and dipole arrangements [61,62]. As illustrated in Figure 2a, the α-phase is the most commonly formed structure during conventional processing and consists of a trans–gauche chain configuration that results in nearly complete dipole cancellation and therefore negligible piezoelectric response [22,63,64]. In contrast, the β-phase exhibits an all-trans molecular conformation in which the dipoles associated with the C–F bonds align along the polymer chain, producing a strong net

polarization and making this phase primarily responsible for piezoelectric behavior in PVDF [22,63,65]. The γ-phase possesses partial polarity but generally produces weaker electromechanical response compared to the β-phase [22,66]. Because of this, maximizing the formation and stability of the β-phase has become a major focus in the development of PVDF-based piezoelectric materials [67,68]. The piezoelectric performance of PVDF also depends on the degree of dipole alignment within the crystalline domains, which can be achieved through electrical poling or through processing methods that induce molecular orientation [68,69]. As shown in Figure 2b, the transformation from the nonpolar α-phase to the polar β-phase can be induced through several processing strategies, including mechanical stretching, thermal treatment, electrical poling, and filler incorporation, all of which promote chain alignment and enhance dipole orientation [68–71]. Techniques such as mechanical stretching, electrospinning, and extrusion have been widely reported to promote chain alignment and enhance β-phase formation [68,69,72]. In additive manufacturing processes such as direct ink writing (DIW), shear forces generated during extrusion can promote molecular orientation in a manner analogous to mechanical stretching, thereby facilitating β-phase formation without requiring extensive post-processing [68–71]. This processing–structure relationship directly influences the electromechanical response observed in functional devices, as illustrated in Figure 2c.

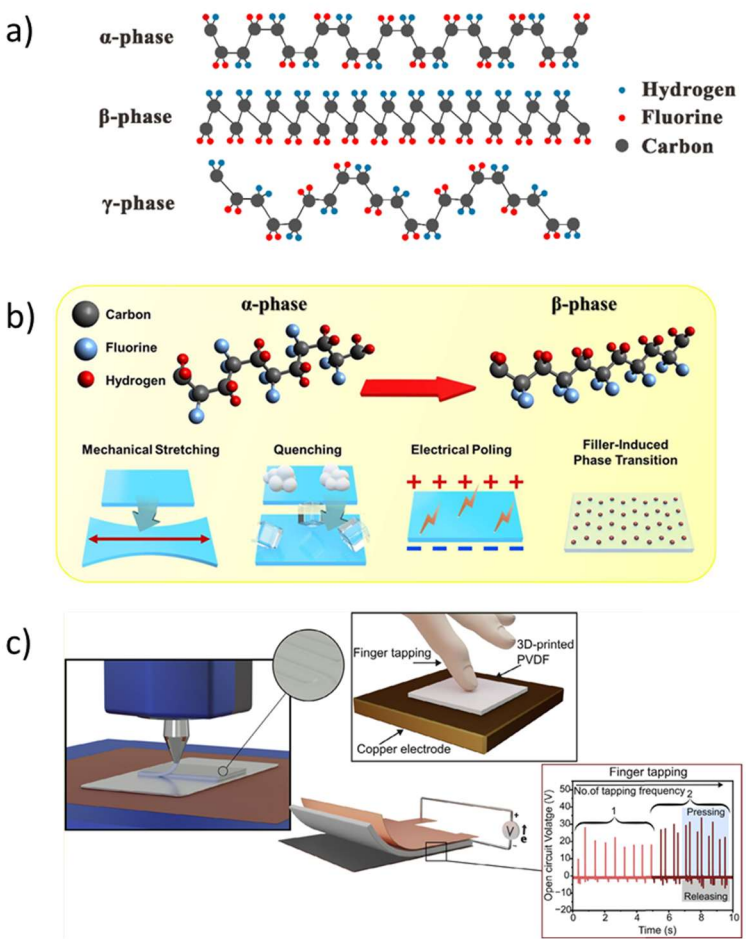


Fig. 2: (a) Molecular conformations of α-, β-, and γ-phases of PVDF [63]. (b) Schematic illustration of α-to-β phase transition induced by mechanical stretching, quenching, electrical poling, and filler incorporation, leading to dipole alignment [72]. (c) Example of a flexible PVDF-based piezoelectric sensor fabricated via direct ink writing, demonstrating voltage generation under cyclic mechanical loading [73].

2.2 Filler-Based Composite Behavior

Polymer composites containing dispersed fillers are widely used to tailor mechanical, electrical, and functional properties beyond those achievable with neat polymers [74,75]. The incorporation of micro- or nanoscale fillers into polymer matrices enables modification of stiffness, density,

electrical conductivity, thermal behavior, and electromechanical response, depending on the characteristics of the filler and its interaction with the surrounding matrix [33,76]. In piezoelectric polymer systems, fillers may also enhance stress transfer, influence dipole alignment, and modify the internal microstructure of the composite, thereby affecting overall performance [33,68,77]. The behavior of filler-reinforced polymer systems is governed by several key factors, including filler concentration, interfacial interactions between the filler and matrix, and the degree of particle connectivity within the composite [76,78]. These factors collectively influence stress transfer, microstructural evolution, and the emergence of functional properties at the macroscale, making their understanding essential for the design and optimization of polymer composites with tailored mechanical and electromechanical performance [33,79]. The following sections examine the effects of filler loading, interfacial interactions, and filler network formation in greater detail.

2.2.1 Filler Loading Effects

The concentration of filler material within a polymer matrix plays a critical role in determining the overall behavior of composite systems [80]. At low filler concentrations, particles are typically well dispersed and act as isolated inclusions within the polymer matrix, leading to localized modifications in stiffness and stress distribution [81]. As filler loading increases, the likelihood of particle–particle interactions rises, significantly influencing the mechanical, electrical, and functional properties of the composite [82]. In many systems, increasing filler content enhances stiffness and improves load transfer between the matrix and reinforcing particles [83,84]. However, excessive filler loading introduces several challenges, including particle agglomeration, increased viscosity during processing, and reduced dispersion uniformity [82,84]. These effects negatively impact processability and can limit achievable performance improvements [81,84].

In piezoelectric polymer composites, filler loading must therefore be carefully balanced to maximize electromechanical response while maintaining sufficient mechanical flexibility and printability [85]. This behavior is often non-monotonic, with an optimal filler concentration yielding the highest electrical output. As filler content increases, improved particle interactions and stress transfer enhance voltage generation. Beyond a critical threshold, however, agglomeration and reduced dispersion quality lead to diminished performance. This non-monotonic behavior is commonly observed in piezoelectric composite systems and is illustrated in Figure 3a, which shows the evolution of electrical conductivity with increasing filler content, and Figure 3b, which demonstrates the corresponding variation in electrical output with filler loading [86,87].

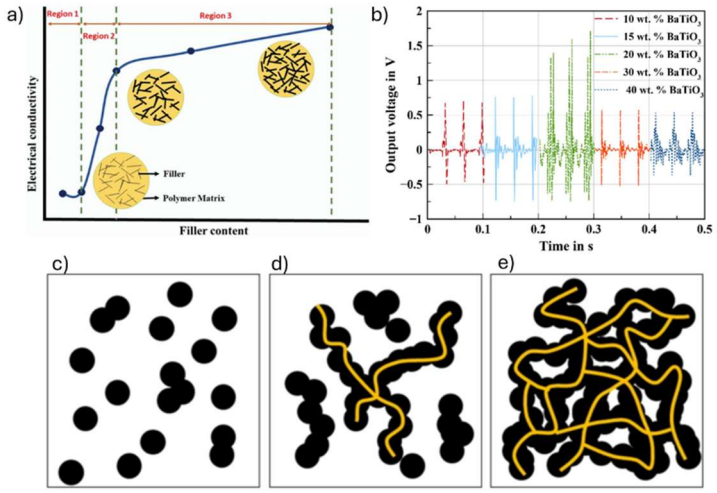


Fig. 3: (a) Schematic representation of electrical conductivity evolution with increasing filler content, highlighting the transition from isolated particles to percolated networks [86]. (b) Representative output voltage signals for composites with varying filler loadings, demonstrating an optimal concentration for maximum electrical response [87]. (c–e) Evolution of filler microstructure with increasing loading: (c) isolated particles, (d) partially connected clusters, and (e) fully percolated network [88].

2.2.2 Interfacial Interactions and Network Formation

Beyond filler concentration, the nature of interfacial interactions between particles and the surrounding polymer matrix plays a critical role in determining composite performance [89]. Strong interfacial adhesion promotes efficient stress transfer, allowing mechanical deformation of the matrix to be effectively transmitted to the embedded fillers, which is particularly important in piezoelectric systems where electromechanical coupling depends on local strain transfer [40,89]. At low filler loadings, particles remain largely isolated with minimal interaction, limiting the formation of continuous pathways for stress or charge transfer. As filler content increases, particles begin to interact through physical contact or polymer-mediated bridging, enabling the formation of interconnected networks that enhance both mechanical reinforcement and electrical response [89,90]. This transition is illustrated in Figure 3c–e, where the system evolves from isolated particle dispersion (Figure 3c) to the formation of localized conductive or stress-transfer pathways (Figure 3d), and ultimately to a percolated network structure (Figure 3e) [88]. While these networks improve functional performance, excessive connectivity or poor dispersion can lead to agglomeration and non-uniform stress distribution, which may negatively affect both mechanical integrity and electromechanical efficiency [82,91].

2.3 Lightweight Filler Architectures

Lightweight composite architectures have gained increasing attention for applications requiring reduced density without sacrificing mechanical functionality, particularly in aerospace, transportation, and flexible systems [92,93]. A common strategy involves incorporating hollow fillers into polymer matrices, introducing internal void space that lowers bulk density while maintaining load transfer through the surrounding matrix [29,94]. Beyond density reduction, these fillers can also influence deformation behavior and stress distribution, making them a versatile

design tool for multifunctional composites. As a result, lightweight filler architectures have emerged as an effective approach for tailoring both structural and functional performance in polymer systems.

2.3.1 Hollow Microspheres and Density Reduction

Hollow microspheres are commonly used as fillers in polymer composites to reduce density while maintaining structural integrity within the material [29,94]. These particles typically consist of thin-walled spherical shells enclosing an internal gas-filled cavity, which introduces controlled porosity into the composite system [95]. When dispersed within a polymer matrix, hollow microspheres reduce the bulk density of the material while still allowing the surrounding matrix to support mechanical loads [96]. Glass microspheres are particularly attractive for lightweight composite applications because they offer relatively high compressive strength, chemical stability, and compatibility with a wide range of polymer matrices [94,95]. In addition to single-filler systems, recent studies have explored hybrid filler architectures that combine hollow particles with reinforcing phases such as fibers to simultaneously tailor density and mechanical performance [29,97]. The degree of density reduction achievable in these systems depends on filler type and volume fraction; as shown in Figure 4e, composite density decreases with increasing filler volume fraction [97].

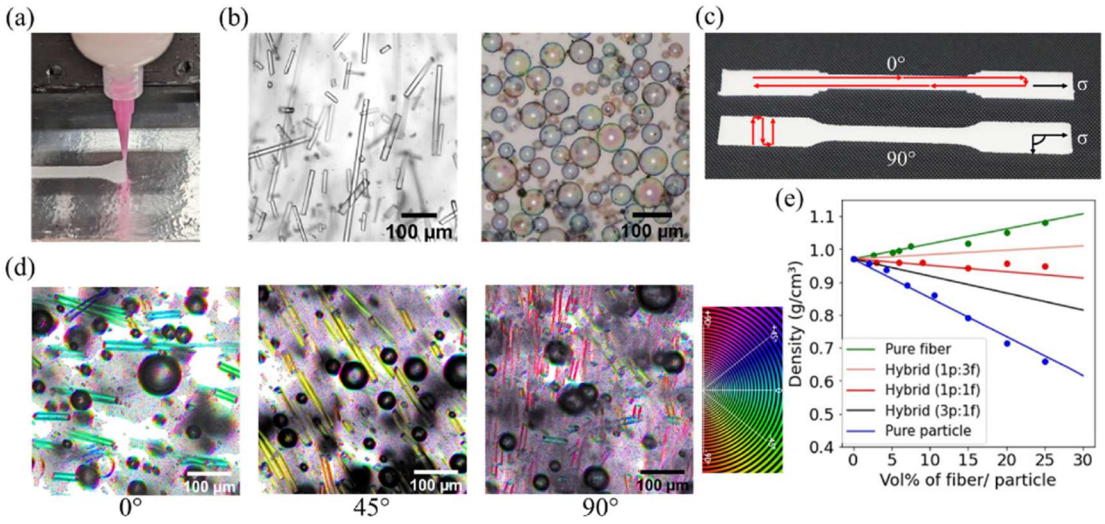


Fig. 4: Direct ink writing (DIW) fabrication and structure–property relationships of hybrid lightweight composites [97]. (a) DIW printing of composite inks into tensile specimens. (b) Representative fillers used in the composites, including glass microfibers and hollow glass microspheres. (c) Printed specimens with different printing directions (0° and 90°). (d) Microstructures of printed composites at 0°, 45°, and 90° printing directions showing filler distribution and alignment. (e) Composite density as a function of filler volume fraction, comparing theoretical predictions (lines) and experimental measurements (points).

2.3.2 Mechanical Compliance and Energy Absorption

The incorporation of hollow microspheres within polymer matrices can significantly modify the mechanical deformation behaviour of composite systems. Unlike solid fillers, hollow particles introduce localized regions of compliance that influence how stress is distributed throughout the material during mechanical loading [94]. Under compressive or impact loading conditions, microspheres may undergo elastic shell deformation, localized buckling, and progressive collapse depending on their structural characteristics and the properties of the surrounding matrix [94,95]. These deformation mechanisms enable syntactic composites to dissipate mechanical energy more

effectively than many traditional solid-filled materials [96,98]. As shown in Figure 5, the compressive stress–strain response of HGM composites typically exhibits three characteristic regions: an initial elastic stage, a plateau region associated with progressive microsphere collapse, and a densification stage where the material compacts at higher strains [93]. Increasing the microsphere volume fraction generally reduces the peak compressive stress while extending the plateau region, indicating a greater contribution of microsphere deformation to energy absorption [93]. Due to this behavior, hollow microsphere composites have been widely investigated for applications requiring energy absorption, vibration damping, and impact resistance [29–31]. In soft polymer matrices such as elastomers and silicones, the interaction between microsphere deformation and matrix elasticity can further enhance strain tolerance and recoverability, making syntactic composites attractive for multifunctional lightweight materials that require both structural performance and mechanical adaptability [96,98].

.

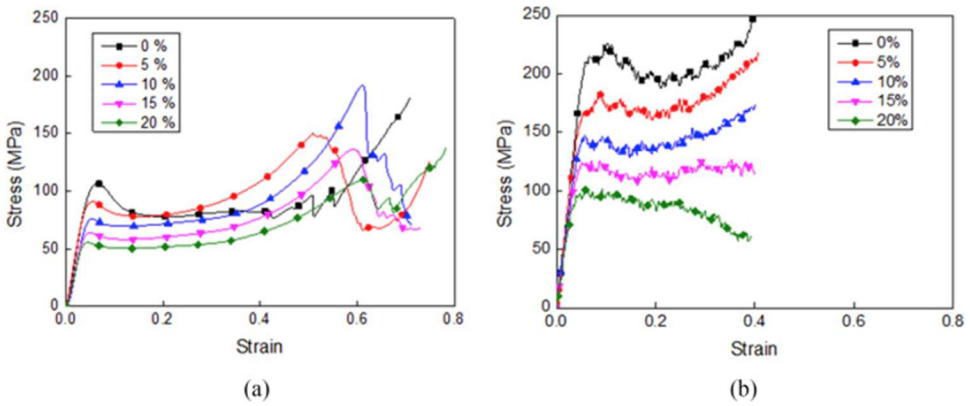


Fig. 5: Compressive stress–strain behaviour of HGM filled polymer composites at different microsphere volume fractions under (a) quasi-static and (b) dynamic loading conditions [93].

2.4 DIW Processing and Network Effects

Additive manufacturing techniques have increasingly been explored for the fabrication of functional polymer composites with tailored architectures and properties [33,34,77]. Among these approaches, direct ink writing (DIW) has emerged as a versatile method for printing soft materials, particle-filled inks, and viscoelastic polymer systems [33,34,77]. DIW relies on the extrusion of shear-thinning inks through a nozzle, allowing materials to be deposited layer-by-layer to form complex three-dimensional structures [99]. The rheological behaviour of the printing ink plays a crucial role in determining print fidelity, particle dispersion, and the resulting microstructure of the printed material [35,100]. In particle-filled polymer systems, the extrusion process can also influence filler orientation, particle interactions, and the development of particle networks within the composite [68–71]. Consequently, the processing conditions used during DIW can significantly affect both the internal structure and the resulting mechanical and functional properties of the printed material [33,34,77].

2.4.1 Rheology and Shear Alignment

The rheological properties of composite inks are critical for successful DIW processing and strongly influence the resulting material structure after printing [35,100]. To be printable, DIW inks must typically exhibit shear-thinning behavior, where viscosity decreases with increasing shear rate during extrusion but rapidly recovers once deposited, enabling the material to flow through the nozzle while maintaining structural stability after printing [99]. As illustrated in Figure 7, DIW processing involves a combination of rheological requirements including shear-thinning behavior during extrusion, rapid modulus recovery associated with gelation after deposition, and sufficient yield stress to support the weight of subsequently deposited layers [99,101]. These rheological transitions allow the material to transition from a flowing state inside the nozzle to a

structurally stable filament once printed [99]. In particle-filled inks, the shear forces generated during extrusion can also influence particle orientation and distribution within the polymer matrix [68–71]. Elongated or anisotropic fillers often align along the direction of shear, creating anisotropic microstructures that influence mechanical and functional performance [68–71]. Even in systems containing spherical particles, shear flow can affect particle packing and dispersion within the ink, making control of rheological properties and shear conditions essential for achieving consistent microstructures and reliable composite performance [35,100].

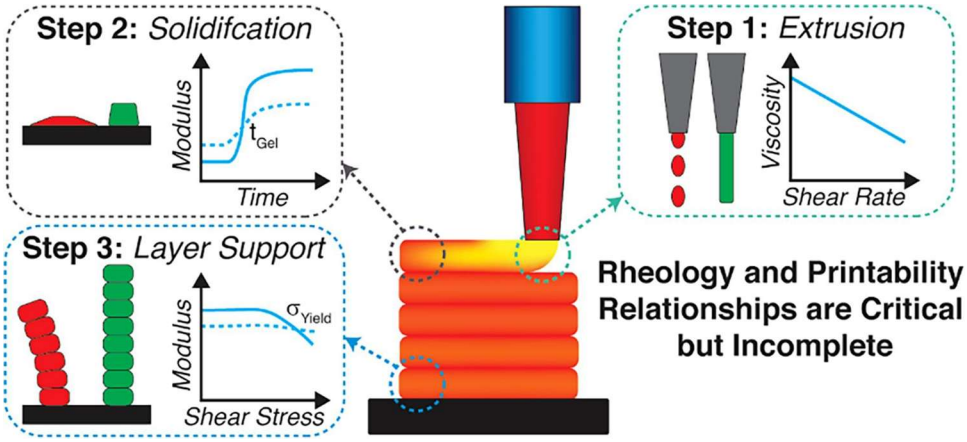


Fig. 6: Schematic illustration of rheological requirements for DIW, showing shear-thinning behavior during extrusion, gelation-driven modulus recovery after deposition, and yield stress required for layer support during printing [101].

Chapter 3: Materials and Experimental Methods

3.1 Materials

PVDF powder and N-methyl-2-pyrrolidone (NMP) solvent were used to prepare the coating solution for functionalizing HGMs. The HGMs (FibreGlast® 22) served as lightweight structural fillers within the composite system. Polydimethylsiloxane (PDMS) systems, SE 1700 and Sylgard 184, were used as the elastomeric matrix materials. Copper tape was used as compliant electrodes during electromechanical testing to enable voltage measurement under mechanical loading. For dynamic testing applications, commercial foam earplugs (3M, Inc.) were used as substrates for integrating printed composite films. All materials were used as received without further modification unless otherwise specified.

3.2 Preparation of PVDF-Coated Hollow Glass Microspheres

PVDF-coated HGMs were prepared using a solution-based coating process to promote uniform polymer coverage and minimize particle agglomeration. PVDF powder was first dissolved in NMP at a 1:10 weight ratio to form a homogeneous coating solution. HGMs were then introduced into the solution at a solvent-to-particle ratio of 1:3 by weight and mixed using a FlackTek SpeedMixer at 3000 rpm for 5 minutes to ensure uniform dispersion. Following mixing, the suspension was subjected to ultrasonication at 80 °C for 45 minutes with the container lid open to facilitate solvent evaporation and improve coating uniformity on the particle surfaces. The coated microspheres were subsequently dried in an oven at 80 °C for at least 24 hours to remove any remaining solvent. This process resulted in PVDF-coated HGMs with improved dispersion characteristics and enhanced interfacial compatibility within the polymer matrix.

3.3 Composite Ink Preparation

Composite inks were prepared by incorporating PVDF-coated HGMs into a PDMS matrix at different filler loadings. The PDMS base materials, SE 1700 and Sylgard 184, were combined at a 70:30 weight ratio and mixed to form a homogeneous elastomeric matrix. Curing agents were then added at a 1:10 weight ratio relative to each respective base material and mixed until uniform. PVDF-coated HGMs were subsequently added to the PDMS formulation at 0 (pure PDMS), 5, 10, 15, 20, and 25 wt% and mixed using a speed mixer at 3000 rpm for 3 min to promote uniform particle dispersion. The prepared composite inks were then used for rheological characterization prior to further processing.

3.4 Rheological Characterization of Inks

The rheological behavior of the composite inks was characterized to evaluate their suitability for DIW. Measurements were performed using an Anton Paar MCR 302 rheometer equipped with a cone-plate geometry (CP25-1, 25 mm diameter, 1° cone angle). The zero gap was set to 0.05 mm prior to testing to ensure consistent sample loading conditions. Frequency sweep tests were conducted to assess the viscoelastic response of the inks, with particular focus on storage modulus and loss modulus across varying angular frequencies. These measurements were used to evaluate shear-thinning behavior and viscoelastic properties relevant to extrusion and shape retention during printing. Following rheological testing, the inks were transferred into 10 mL Luer-lock syringes and centrifuged at 3000 rpm for 5 min to remove trapped air and prepare the material for direct ink writing.

3.5 Direct Ink Writing (DIW) Fabrication

Composite specimens (15 × 15 × 4 mm³, L × W × H) were 3D printed on a Hyrel® (3D Engine SR) platform through a nozzle with an inner diameter of 410 μm. Three-dimensional CAD models were created in SolidWorks® and imported into slicing software (Slic3r®) to generate G-code consisting of alternating 0°/90° linear infill toolpaths between successive layers. Prior to printing, ink-filled 10 mL Luer-lock syringes were mounted and purged to remove residual air. The nozzle height was set to zero relative to the build surface to ensure consistent first-layer extrusion. Printing was carried out using a layer height of 290 μm on a glass substrate covered with Bytac® FEP-coated aluminum foil to facilitate sample removal after curing. Prints were executed at a travel speed of 15 mm/s under ambient laboratory conditions, with continuous extrusion to maintain uniform filament width and consistent overlap between adjacent lines. Following fabrication, the samples were left on the build platform to minimize handling-induced distortion and were then cured in an oven at 80 °C for 24 hours.

3.6 Mechanical and Electromechanical Testing

Cyclic compressive tests with simultaneous voltage output measurements were performed to evaluate the electromechanical response of the 3D printed composites. All compression experiments were conducted using a Mark-10® test frame under displacement-controlled loading at a constant crosshead speed, with samples positioned between two parallel compression plates. Prior to testing, copper tape was applied to the top and bottom surfaces of each specimen to serve as electrodes for voltage measurement. The specimens were carefully centered and brought into gentle contact with the plates to ensure proper alignment and parallelism. Each sample underwent 10 repeated cyclic compression tests, with the maximum displacement selected to achieve approximately 30% engineering strain relative to the initial specimen height. The nominal strain

rate was approximately 0.3 s^{-1}, determined from the applied crosshead speed and specimen thickness. Force and displacement data were recorded throughout testing for subsequent stress–strain analysis. The electrodes were connected to a Siglent SDM3045X digital multimeter (Siglent Technologies, Shenzhen, China), enabling real-time acquisition of voltage signals during cyclic loading. Mechanical and electrical data were collected simultaneously to allow direct correlation between compressive behavior and the resulting piezoelectric voltage response across different composite formulations.

3.7 Thermal Characterization

Thermal characterization was conducted to evaluate the stability and heat transfer properties of the composite materials as a function of filler loading. These measurements provide insight into thermal degradation behavior, heat capacity, and thermal conductivity, which are critical for understanding material performance under varying environmental conditions. A combination of thermogravimetric analysis (TGA), thermal conductivity measurements, and differential scanning calorimetry (DSC) was used to fully characterize the thermal response of the printed composites.

3.7.1 Thermogravimetric Analysis (TGA)

Thermogravimetric analysis was performed on pure PDMS and composite samples containing 5 wt% and 15 wt% PVDF-coated HGMs using a TGA5500 (TA Instruments, New Castle, DE, USA) with standard 100 µL platinum pans. Samples were heated from room temperature to 800 °C at a rate of 10 °C/min under a nitrogen atmosphere with a flow rate of 25 mL/min. The mass loss behavior was recorded as a function of temperature to assess thermal stability and decomposition characteristics of the composites. These measurements were used to compare degradation onset temperatures and residual mass fractions across different filler loadings.

3.7.2 Thermal Conductivity

Thermal conductivity was measured using a Measurement Platform-2 (MP-2) TPS-4 system (Thermtest Instruments, Fredericton, NB, Canada) based on the transient plane source (TPS) method. In this technique, a controlled heat pulse is applied through a sensor in contact with the sample, and the resulting transient temperature response is recorded to determine thermal conductivity. Solid samples with dimensions suitable for the TPS sensor were used to ensure accurate measurements. All tests were conducted under ambient conditions, and consistent sample preparation was maintained to allow comparison between compositions.

3.7.3 Differential Scanning Calorimetry (DSC)

Specific heat capacity measurements were conducted using a Differential Scanning Calorimeter (DSC 4000, PerkinElmer, Waltham, MA, USA). Samples with masses between 5 and 10 mg were sealed in aluminum pans and heated at a rate of 10 °C/min over the desired temperature range. The heat flow was recorded as a function of temperature, and specific heat capacity values were determined from the measured response. These measurements were used to evaluate the thermal energy storage behavior of the composites and assess how filler incorporation influences heat capacity.

3.8 Dynamic Mechanical Analysis (DMA)

Dynamic mechanical analysis (DMA) was performed to evaluate the viscoelastic behavior of the composite materials as a function of frequency and temperature. Measurements were conducted using a TA Instruments RSA-G2 dynamic mechanical analyzer equipped with tension clamps. Rectangular specimens were tested under oscillatory loading conditions to obtain storage modulus, loss modulus, and damping behavior. Frequency sweep tests were performed over a range of

angular frequencies to characterize the rate-dependent mechanical response of the materials. Temperature-dependent behavior was also evaluated by conducting tests from 25 °C to 100 °C in 5 °C increments under a nitrogen atmosphere to minimize oxidative effects. Time-temperature superposition (TTS) was applied to generate master curves, enabling the extension of viscoelastic behavior over a wider frequency range. A reference temperature of 40 °C was selected, and shift factors were determined to align individual frequency sweeps into a continuous master curve. The Williams-Landel-Ferry (WLF) equation was used to model the temperature dependence of the shift factors and to quantify the viscoelastic response of the composites. These measurements provide insight into the influence of filler loading on stiffness, energy dissipation, and long-term mechanical performance.

3.9 Dynamic Testing (Impact and Blast)

Dynamic testing was conducted to evaluate the response of the composite materials under transient loading conditions representative of impact and pressure-driven events. These tests provide insight into the material behavior under rapid deformation and their potential for sensing and energy absorption in dynamic environments. Two testing methods were employed, including drop testing and blast testing, to capture both low-velocity impact and high-rate pressure loading responses.

3.9.1 Drop Testing

Drop testing was performed to assess the electromechanical response of the composites under repeated impact loading. Samples were subjected to controlled drop heights, and the resulting voltage signals were recorded to evaluate the relationship between impact energy and electrical output. The tests were conducted by releasing a mass from specified heights onto the sample surface, generating transient compressive loading conditions. Voltage signals were measured in

real time using a digital multimeter, allowing for analysis of peak voltage response and signal consistency across repeated impacts. Multiple trials were conducted for each condition to ensure repeatability and enable comparison between different composite formulations.

3.9.2 Blast Testing

Blast overpressures were generated using a compressed gas-driven blast apparatus housed in an anechoic chamber, following previously established blast characterization protocols [102,103]. A rigid head block was mounted in a fixed holder with its head facing the blast source to ensure consistent alignment across trials. The head block was equipped with a 3D-printed dummy ear and a standard foam earplug (3M, Inc., St. Paul, MN), with the PDMS-HGM film 3D printed on the entrance side, which was inserted into the dummy ear canal. Blast waves were produced by rupturing polycarbonate diaphragms (McMaster-Carr, Atlanta, GA) to generate controlled pressure pulses. Multiple consecutive blast exposures were performed with sufficient time intervals between each test. Pressure data were acquired using a data acquisition system equipped with an analog-to-digital converter (National Instruments, Austin, TX) and were subsequently processed and analyzed using LabVIEW software (National Instruments, Inc.).

Chapter 4: Microstructure, Processing, and Physical Characteristics

The experimental results provide insight into how PVDF-coated HGMs influence the behavior of PDMS-based composites as a function of composition. Building on the fabrication approach described previously, the results are evaluated to determine how the incorporation of coated microspheres affects mechanical response and electromechanical performance. Emphasis is placed on identifying trends in stress–strain behavior, energy dissipation, and voltage generation across different filler loadings. These responses are discussed in relation to the observed dispersion of HGMs within the matrix and the overall uniformity of the composite structure [ref]. The presence of the PVDF coating is also considered in terms of its role in enabling consistent performance and maintaining composite integrity across compositions [ref]. Comparisons between samples highlight the balance between maintaining compliance while enhancing functional response, providing a clearer understanding of the behavior of these lightweight composite systems.

4.1 Microstructural Characterization

Microstructural characterization was conducted to evaluate the morphology, coating quality, and dispersion behavior of the PVDF-coated HGMs prior to incorporation into the PDMS matrix. These observations provide insight into the effectiveness of the coating process and the influence of processing conditions on particle uniformity and surface coverage. SEM and EDS analyses were used to assess coating consistency, particle size distribution, and the presence of interparticle interactions. Understanding these features is important for interpreting how filler characteristics influence the rheological behavior, mechanical response, and electromechanical performance of the resulting composites.

4.1.1 Morphology and Coating of PVDF-Coated HGMs

The morphology of the PVDF-coated HGMs was examined prior to composite fabrication to assess coating quality and particle characteristics. Figures 7 and 8 show representative SEM and EDS images at multiple magnifications, highlighting coating uniformity, individual microsphere morphology, and particle–particle interactions. As shown in Figure 7a–b, the SEM images and corresponding EDS overlays indicate fluorine localized at the microsphere surfaces, consistent with uniform PVDF coverage. The microspheres exhibited a mean particle diameter of 54.2 ± 23.5 μm, indicating a relatively broad size distribution typical of HGMs. The higher magnification image in Figure 8a reveals smooth and continuous PVDF coatings, suggesting effective mixing and consistent surface coverage across individual microspheres, with no significant regions of incomplete coating observed. In addition to coating uniformity, localized interactions between adjacent particles are evident, as shown in Figure 8b, where PVDF capillary bridges are observed between neighboring microspheres, likely formed during solvent evaporation in the particle preparation stage. These features indicate the presence of physical connections between particles and suggest the formation of an interconnected PVDF network. The presence of these interparticle connections is expected to influence particle interactions during subsequent processing, particularly in terms of resistance to flow within the composite inks. Overall, the observed coating uniformity and particle morphology demonstrate that the processing approach was effective in producing consistently functionalized HGMs with minimal agglomeration, providing a stable and uniform foundation for composite fabrication.

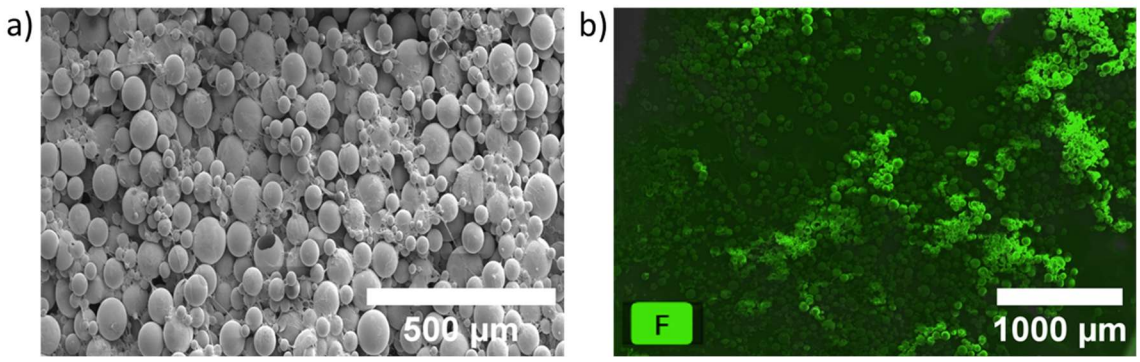


Fig. 7: a) SEM image and b) EDS overlay image highlighting Fluorine of the PVDF-coated HGMs.

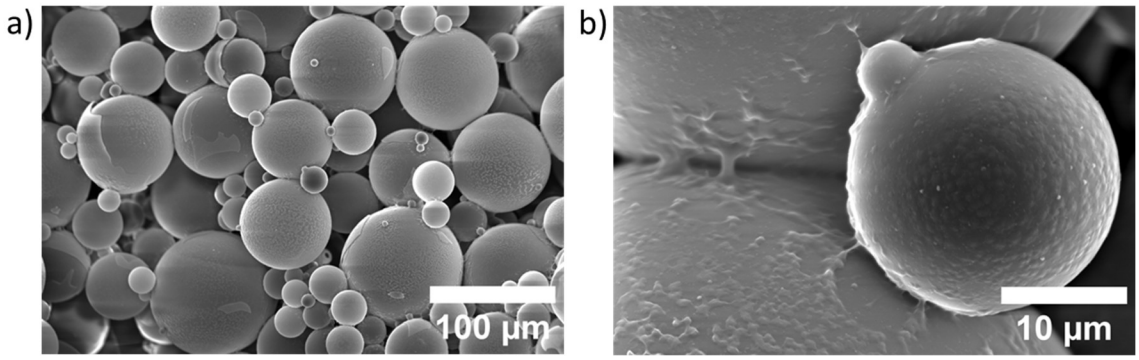


Fig. 8: a) SEM image of uniform coating on HGMs. b) Close-up SEM image showing capillary bridges formation between neighboring microspheres.

4.1.2 Effect of Processing on Coating Uniformity

To further evaluate the influence of processing conditions on coating quality, additional SEM and EDS analyses were performed on samples prepared with and without proper ultrasonication. Representative micrographs and corresponding elemental compositions are shown in Figure 9 and Table 1 for samples processed with ultrasonication, and in Figure 10 and Table 2 for samples prepared without this step. For samples subjected to sufficient ultrasonication, the SEM images (Figures 9a-b) show relatively uniform particle dispersion and consistent surface coverage across the HGMs. The corresponding EDS results (Table 1) indicate fluorine atomic percentages of

approximately 9–11 at% across multiple sites, confirming stable and continuous PVDF coating. In contrast, samples prepared without sufficient ultrasonication exhibit clear differences in both morphology and composition. As shown in Figures 10a-d, these samples display particle clustering, surface irregularities, and nonuniform coating coverage. The corresponding EDS measurements (Table 2) show lower and more spatially variable fluorine content, ranging from approximately 3–6 at%, indicating incomplete coating and inconsistent PVDF distribution. The increased variability in fluorine content across different regions further supports the presence of localized coating deficiencies and particle aggregation. These results demonstrate that ultrasonication plays a critical role in achieving homogeneous PVDF coverage and minimizing microsphere agglomeration during the coating process, which is essential for ensuring consistent composite behavior in subsequent processing and testing.

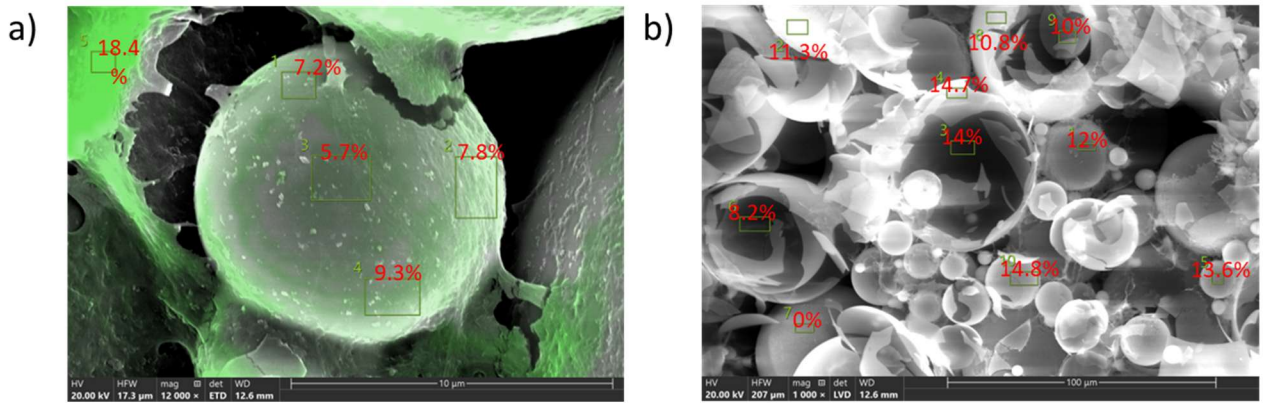


Fig. 9: SEM–EDS images of Sample 1. A) High-magnification micrograph showing localized fluorine content at selected regions. B) Lower-magnification micrograph from a different site showing spatial variation in fluorine distribution across the sample.

Table 1: EDS elemental composition of Sample 1 in Figure S1, showing atomic and weight percentages of fluorine and other primary elements.

Element	Atomic %	Std. Dev.	Weight %	Std. Dev.	Atomic %	Std. Dev.	Weight %	Std. Dev.
	Sample 1 Site A				Sample 1 Site B			
C	10.59	2.29	6.54	1.37	14.52	12.11	9.26	8.83
O	51.56	5.71	42.34	5.15	44.3	8.96	35.32	5.20
F	10.94	4.41	11.24	4.33	9.68	5.04	9.58	6.07
Si	18.75	2.23	3.13	2.55	21.76	5.77	30.32	6.47

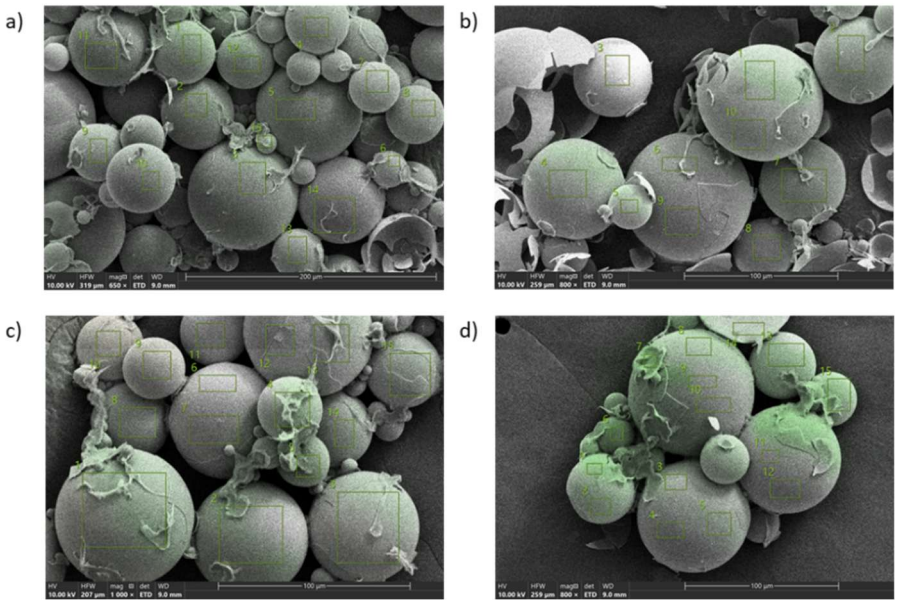


Fig. 10: SEM–EDS images of PVDF-coated HGMs without proper ultrasonication. (a–d) Representative micrographs from different sites of the sample showing particle clustering, nonuniform coating, and surface irregularities. Fluorine detection confirms the presence of PVDF on the HGMs despite incomplete dispersion.

Table 2: EDS elemental composition of Sample 2 in Figure S2, showing atomic and weight percentages of fluorine and other primary elements.

Element	Atomic %	Std. Dev.	Weight %	Std. Dev.	Atomic %	Std. Dev.	Weight %	Std. Dev.
Sample 2 Site A					**Sample 2 Site B**			
C	4.560	4.239	2.300	1.794	3.200	2.721	1.763	1.702
O	56.41	6.456	39.76	6.056	56.51	15.57	37.85	10.69
F	5.587	7.156	4.373	4.767	3.238	2.685	2.688	2.662
Si	22.89	6.933	28.573	8.616	20.66	15.65	25.91	17.68
Sample 2 Site C					**Sample 2 Site D**			
C	7.673	4.404	4.507	2.817	10.23	6.709	6.250	4.324
O	50.46	8.704	38.95	7.132	51.97	8.462	41.33	6.698
F	6.420	6.474	10.64	13.86	5.529	6.416	5.450	6.701
Si	23.25	5.025	31.18	5.069	21.56	6.041	29.74	6.833

4.2 Rheological Behavior

Rheological characterization was performed to evaluate the flow behavior of the composite inks and assess their suitability for direct ink writing. Understanding the rheological response is critical for ensuring stable extrusion, shape retention, and overall print quality, particularly in systems where particle interactions and network formation influence material behavior [35,100]. The incorporation of PVDF-coated HGMs into the PDMS matrix introduces particle–particle interactions that are expected to modify viscosity, shear-thinning behavior, and yielding characteristics, all of which directly govern how the material flows under applied stress and recovers after deposition. In addition to governing flow behavior, during extrusion in direct ink writing, the material experiences high localized shear stresses at the nozzle, which can induce alignment of PVDF molecular chains along the flow direction. This shear-induced alignment acts as a form of mechanical poling, promoting the formation of the electroactive β-phase within the PVDF coating and enhancing dipole orientation and net polarization, thereby reducing or

potentially eliminating the need for conventional electrical poling [68–71]. The viscosity of the composite inks as a function of shear rate is shown in Figure 11a, where all formulations exhibit pronounced shear-thinning behavior, characterized by a significant decrease in viscosity with increasing shear rate. This behavior enables smooth extrusion through the nozzle during printing while maintaining sufficient resistance to flow at low shear rates for shape retention after deposition [99]. Increasing the filler weight fraction from 5 wt% to 25 wt% results in a systematic increase in viscosity across the measured shear rate range, indicating stronger particle–particle interactions and the formation of a more interconnected internal structure within the ink [80,81]. The viscoelastic response of the inks was further evaluated through oscillatory shear measurements, as shown in Figure 11b, where the storage modulus (G′) and loss modulus (G″) are plotted as a function of applied shear stress. At low shear stress, all samples exhibit gel-like behavior, with G′ exceeding G″, indicating a predominantly elastic response governed by the internal particle network [35,100]. As the applied shear stress increases, both moduli decrease and reach a crossover point where G″ exceeds G′, marking the yielding transition from a solid-like to a fluid-like state. This shear-yielding behavior is essential for extrusion-based printing, as it allows the material to flow under the high shear conditions experienced at the nozzle while rapidly recovering its structure once deposited [101]. The observed rheological behavior is consistent with the microstructural features observed in the SEM analysis, where capillary bridges and particle interactions contribute to the formation of a transient network within the composite ink. The practical implications of this behavior are demonstrated in Figure 11c, where consistent extrusion and filament formation are observed during printing, confirming reliable printability across all compositions.

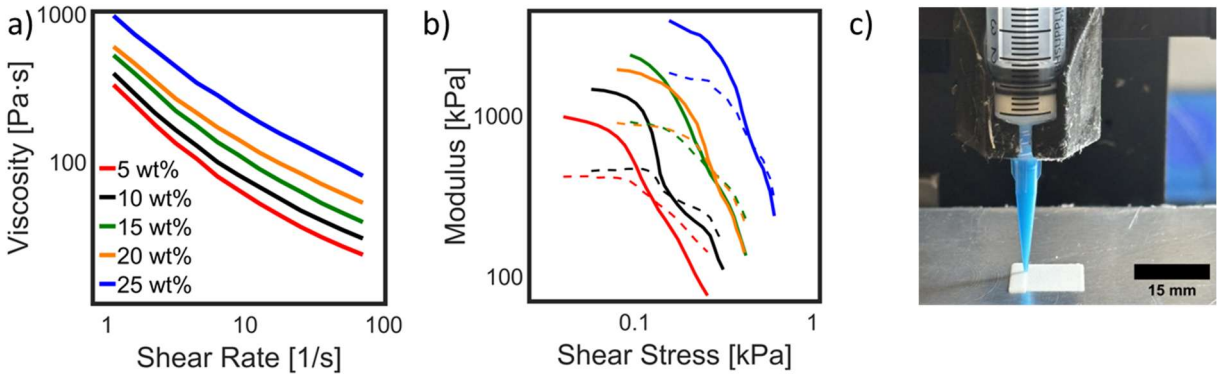


Fig. 11: (a) Measurement of viscosity as a function of shear rate showing shear-thinning behavior across different volume fractions of PVDF-coated HGMs composite inks. (b) Storage (solid) and loss (dashed) moduli against applied shear stress, demonstrating shear yielding behaviors of all inks. (c) 3D printing of composite ink with 15 wt% PDMS-HGMs.

4.3 Density and Structural Characteristics

The bulk density of the cured composites was measured to evaluate the effect of PVDF-coated HGMs on the overall material structure. As shown in Figure 12, the composite density decreases monotonically with increasing filler loading, decreasing from 1.08 ± 0.01 g/cm³ for pure PDMS to 0.57 ± 0.01 g/cm³ at 25 wt% PVDF-coated HGMs, corresponding to an overall reduction of approximately 47%. To further quantify this trend, the experimental density values were fitted using a rule-of-mixtures (ROM) model to estimate the effective density of the PVDF-coated HGM particles. The composite density (ρ_c) was expressed in terms of the matrix density (ρ_M) and filler weight fraction (f_w), accounting for the relative contributions of each phase:

$$\rho_c = \frac{\rho_M f_w}{\rho_M f_w + \rho_f(1-f_w)}\rho_f + \frac{\rho_f(1-f_w)}{\rho_M f_w + \rho_f(1-f_w)}\rho_M \quad (1)$$

where ρ_M represents the density of the PDMS matrix, ρ_f is the effective density of the PVDF-coated HGMs, and f_w is the filler weight fraction. Using this relationship, the effective particle density was determined to be ρ_f = 0.226 ± 0.010 g/cm³, obtained through fitting to the experimental data shown in Figure 12. The agreement between the ROM model and the measured densities indicates that the model provides a reasonable representation of the composite system across the range of filler loadings considered.

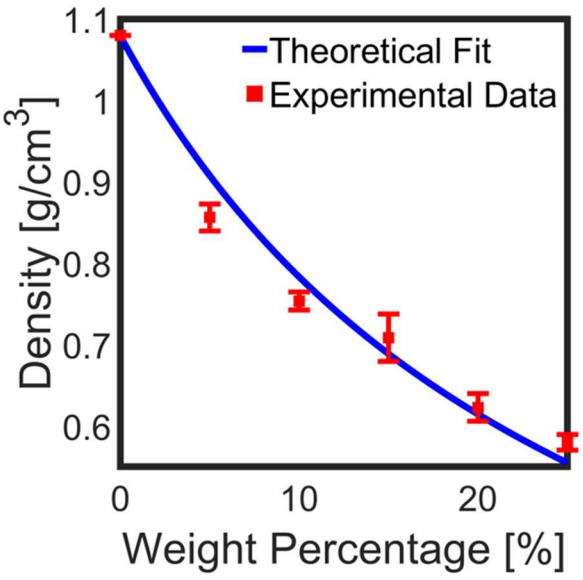


Fig. 12: Experimental data and the theoretical curve of density of cured composites with different filler loading.

To further characterize the coated microspheres, a geometric model was used to estimate the radius of the PVDF-coated HGMs based on density relationships and mass balance:

$$r = \sqrt[3]{\left(\frac{(\rho_{HGM} - \rho_{PVDF}) \cdot r_{HGM}^3}{\rho_f - \rho_{PVDF}}\right)} \quad (2)$$

where the densities of the uncoated HGMs and PVDF were taken as ρ_{HGM}= 0.13 ± 0.05 g/cc and ρ_{PVDF} = 1.78 g/cc, respectively [21,22,97]. Treating the coated microspheres as concentric spheres, the outer radius was determined using the average radius of the uncoated particles (r_{HGM} = 27.1 μm), and the corresponding coating thickness was calculated as $t_{coat} = r - r_{HGM}$, yielding a value of 481 ± 252 nm. The variation in coating thickness is consistent with the distribution of particle sizes and coating characteristics observed during microstructural analysis. These results provide a quantitative description of the composite structure and confirm the effect of increasing filler content on the measured density.

Chapter 5: Mechanical, Functional, and Thermal Performance

5.1 Mechanical Behavior

The mechanical response of the PVDF-coated HGM composites was evaluated under cyclic compressive loading to assess the influence of filler incorporation on stiffness, deformation behavior, and energy absorption characteristics. Understanding the mechanical behavior of these composites is critical for applications requiring lightweight materials that can sustain repeated deformation while maintaining structural integrity and functional performance [34,90]. The introduction of hollow microspheres into the PDMS matrix modifies load transfer mechanisms and alters the effective stiffness of the composite by introducing compliant regions associated with the hollow structure [66,72]. In addition, the interaction between the polymer matrix and the dispersed microspheres contributes to the overall deformation behavior under applied stress, influencing both recoverability and energy dissipation during cyclic loading [80,81]. Cyclic compression testing provides insight into how the composite structure responds to repeated loading conditions and establishes a direct relationship between filler content and mechanical performance, forming the basis for subsequent analysis of constitutive behavior and energy absorption capability.

5.1.1 Cyclic Stress-Strain Behavior

Cyclic compressive tests were performed on the 3D-printed specimens to evaluate their mechanical stability and deformation response under repeated loading. A representative stress–strain response for the 15 wt% composite over 10 cycles is shown in Figure 13, where the first loading cycle exhibits higher stiffness and peak stress compared to subsequent cycles, indicating an initial rearrangement or settling of the internal microstructure under applied load [80,81].

Following this initial cycle, the stress–strain curves stabilize and overlap across subsequent cycles, demonstrating repeatable mechanical behavior and structural consistency under cyclic deformation. The hysteresis observed between the loading and unloading paths, represented by the shaded region in Figure 13, corresponds to the mechanical energy dissipated during each cycle. This stabilized cyclic response indicates that the composite structure is capable of sustaining repeated compressive loading without significant degradation in mechanical performance, which is important for applications involving dynamic or repeated mechanical stimuli.

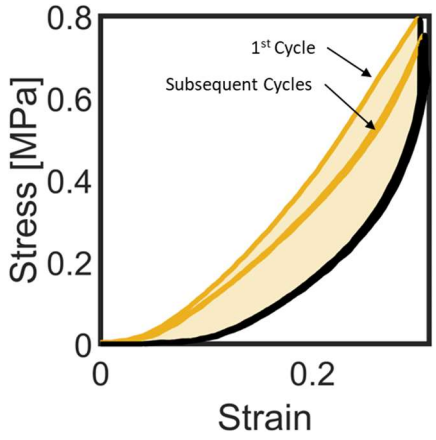


Fig. 13: Representative cyclic stress–strain curve of a 3D-printed PDMS–HGM composite (15 wt%), with the shaded region indicating mechanical energy hysteresis during compressive cycles

5.1.2 Specific Stress and Energy Absorption

The effect of filler incorporation on mechanical performance was further evaluated through comparison of the specific stress–strain behavior and energy absorption characteristics of the composites. As shown in Figure 14a, all PDMS–HGM composites exhibit lower peak specific stress compared to pure PDMS at compressive strains up to 30%, indicating a reduction in stiffness and an increase in compliance with increasing filler content. The 15 wt% composite demonstrates a 22.1% decrease in peak specific stress relative to pure PDMS, while further reductions are

observed at higher filler loadings, reaching up to 49.2% for the 25 wt% composite. This progressive softening behavior is associated with the incorporation of hollow microspheres, which reduce the effective load-bearing cross-section and alter stress distribution within the matrix [66,72]. At higher filler contents, additional reductions in stiffness are influenced by nonuniform particle dispersion and localized agglomeration, which can affect load transfer and promote localized deformation under compressive loading [80,81]. As a result of this increased compliance, the composites exhibit significantly enhanced energy absorption capabilities, as shown in Figure 14b, where all composite formulations demonstrate higher specific energy absorbance compared to pure PDMS across the investigated stress range. At an applied stress of 300 kPa, the composites achieve approximately 2.9 to 4.3 times the specific energy absorbance of the unfilled polymer. This behavior highlights the ability of the PVDF–HGM composites to dissipate mechanical energy more effectively while maintaining structural integrity, supporting their suitability for applications requiring lightweight materials with high energy absorption capacity.

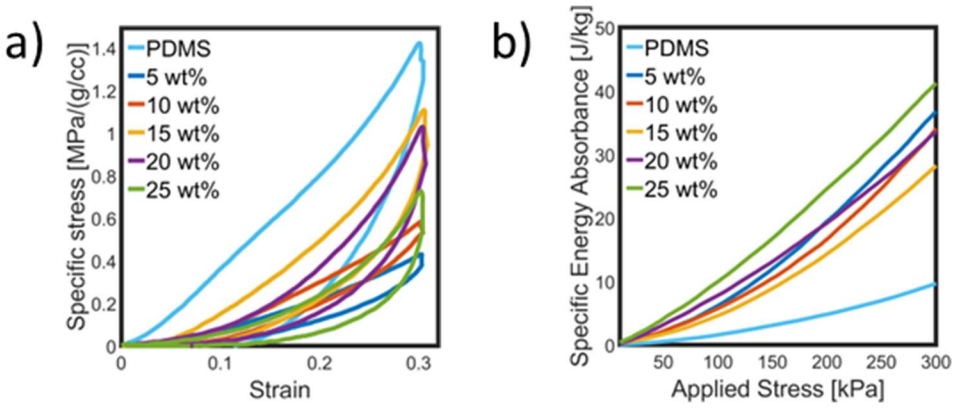


Fig. 14: (a) Specific stress–strain behavior of all specimens up to 30% strain, (b) specific energy absorption as a function of applied compressive stress for different specimens.

5.1.3 Hyperelastic Modeling

To characterize the nonlinear mechanical response observed in the stress–strain behavior, a second-order polynomial hyperelastic model was employed to describe the material deformation. As shown in Figure 15, all composites exhibit a superlinear stress–strain relationship, indicating nonlinear elastic behavior typical of elastomeric materials under finite deformation. To quantify this behavior, a second-order polynomial hyperelastic model was used, in which the strain energy density function $U$was expressed in terms of the first and second invariants of deformation [104], allowing the model to capture both deviatoric and volumetric contributions to the material response:

$$U = \sum_{i+j=1}^{2} C_{ij}(\bar{I}_1 - 3)^i(\bar{I}_2 - 3)^j + \frac{1}{D_1}(J-1)^2 \quad (3)$$

where the coefficients C_{ij} define the shear response of the material, while D_1 governs compressibility, and the invariants $\bar{I}_1$, $\bar{I}_2$, and the elastic volume ratio J describe the deformation state. The fitted material parameters for the different composite formulations are summarized in Table 3. The hyperelastic model demonstrates strong agreement with the experimental stress–strain data across the full range of applied strains, indicating that the second-order formulation is sufficient to capture the nonlinear behavior of both the pure PDMS and the PVDF–HGM composites. The consistency of the model fit across different filler loadings further suggests that the deformation mechanisms remain governed by elastomeric behavior.

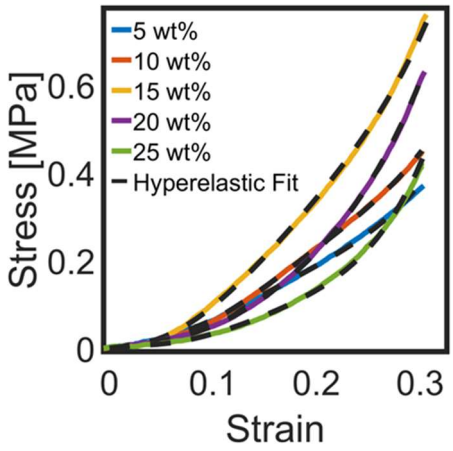


Fig. 15: Comparison of experimental stress–strain responses and second-order polynomial hyperelastic model fits for composites with varying filler contents.

Table 3: Material parameters for the second-order polynomial hyperelastic model of PDMS and the composites with different weight fractions of PVDF-coated HGMs.

Strain Energy Parameters [MPa]						
Weight %	**C_{10}**	**C_{01}**	**C_{20}**	**C_{11}**	**C_{02}**	**D_1**
0%	10.6	-10.4	-64.2	174	-122	0.506
5%	-0.208	0.265	40.3	-98.7	61.4	1.83
10%	-1.54	1.617	53.0	-134	86.9	1.40
15%	-0.355	0.398	61.5	-152	96.5	2.45
20%	-1.44	1.53	40.7	-98.6	62.0	1.22
25%	-1.93	2.00	72.5	-175	109	1.50

5.1.4 Morphological Analysis After Deformation

Following compressive testing, SEM imaging was conducted to assess microstructural changes within the composites, with emphasis on HGM integrity and particle–matrix interactions within the PDMS matrix. As shown in Figure 16a, the uncoated HGMs embedded in the matrix exhibit noticeable structural damage after loading, while the magnified view in Figure 16b reveals severe shell fracture and the presence of surface debris. These features indicate that the thin-walled

microspheres are highly susceptible to damage under compressive stress, leading to localized stress concentrations at the particle–matrix interface that can disrupt effective load transfer. In contrast, the PVDF-coated HGMs shown in Figure 16c display significantly improved structural integrity, with fewer fractured particles and reduced surface damage across the composite. The zoomed-in image in Figure 16d further highlights an individual coated particle maintaining a smooth and continuous surface with minimal deformation, indicating improved shape retention under loading. This behavior suggests that the PVDF coating provides mechanical stabilization of the microsphere surface while enhancing interfacial interaction with the PDMS matrix. As a result, debonding and interfacial slip are reduced, allowing for more efficient stress transfer between the matrix and filler phases [81]. These observations are consistent with the mechanical trends discussed previously, where increased compliance and enhanced energy absorption are associated with the presence of structurally stable, well-integrated microspheres within the composite.

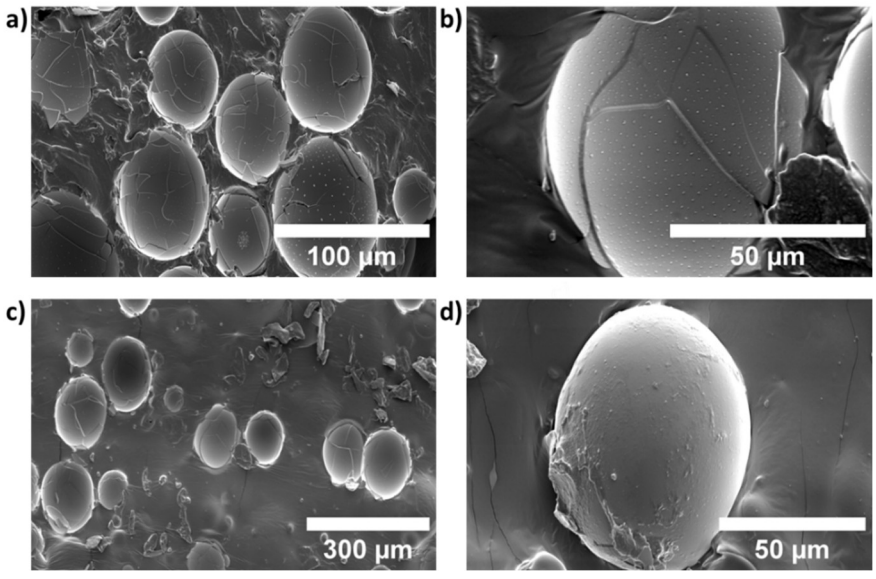


Fig. 16: SEM images after cyclic compressive tests showing (a) uncoated HGMs in the PDMS matrix and (b) a zoom-in view of an uncoated HGM, and (c) PVDF-coated HGMs embedded in the PDMS matrix and (d) a zoomed-in view of an individual coated HGM.

5.2 Electromechanical Response

Electromechanical testing was conducted to evaluate the voltage response of the composites under cyclic compressive loading. As shown in Figure 17a, all specimens generate measurable voltage signals during deformation, with the output amplitude increasing as the filler content increases up to 15 wt%. Beyond this concentration, a reduction in voltage response is observed for the 20 wt% and 25 wt% composites. This trend indicates that intermediate filler loading provides more effective electromechanical coupling, while higher filler concentrations reduce performance due to factors such as particle agglomeration and reduced matrix continuity, which can limit charge transfer and mechanical interaction within the composite [40,87].

To quantify the piezoelectric response, the piezoelectric voltage coefficient g_{33} was calculated based on the measured voltage output, applied load, and specimen geometry:

$$g_{33} = \frac{VA}{Ft} \tag{4}$$

where V represents the measured voltage amplitude with the baseline response of the pure PDMS sample removed, $A$is the effective electrode area, F is the applied compressive load, and t is the specimen thickness. The calculated g_{33} values are presented in Figure 17b, where a similar trend is observed, with the piezoelectric response increasing with filler loading up to 15 wt% and reaching a maximum value of 34.9 ± 1.9 mV·m/N, followed by a decrease at higher concentrations. This result indicates that moderate filler loading is most effective for enhancing piezoelectric sensitivity in the present composite system.

The observed peak in electromechanical performance at intermediate filler content is consistent with trends reported in polymer-based piezoelectric composites, where improved response is associated with enhanced electromechanical interaction at moderate filler loadings and diminished

performance at higher concentrations due to structural and interfacial limitations . The results are also consistent with the XRD analysis shown in Figure 17c, where increased β-phase intensity is observed at 15 wt% compared to higher filler loadings, indicating a greater presence of the electroactive phase at intermediate compositions. At higher filler concentrations, reduced β-phase content suggests disruption of polymer chain organization, which can limit dipole alignment and reduce the efficiency of stress-induced polarization. Overall, these results demonstrate that the electromechanical response of the composites is strongly dependent on filler concentration, with 15 wt% providing the optimal balance between structural integrity and piezoelectric performance.

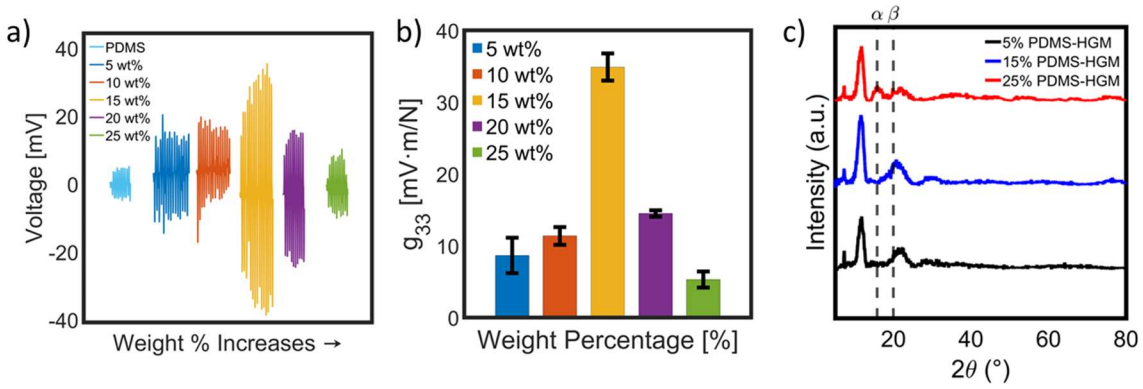


Fig. 17: Electromechanical and structural characterization of PDMS–HGM composites: (a) voltage output measured during cyclic compressive loading and (b) piezoelectric voltage constant g_{33} for composites with increasing PVDF–HGM weight fraction; (c) XRD spectra of PDMS–HGM composites with varying filler contents (5, 15, and 25 wt%), showing diffraction peaks corresponding to the α-phase and β-phase.

5.3 Dynamic Mechanical Analysis

Dynamic mechanical analysis (DMA) was conducted to evaluate the rate-dependent viscoelastic behavior of the composites and to examine how filler loading influences their dynamic mechanical response. Temperature-dependent frequency sweep measurements were performed for pure PDMS, 5 wt%, and 15 wt% composites over an angular frequency range of 1 to 100 rad s^{-1} and a temperature range of 25 to 100 °C. The results show that pure PDMS exhibits higher storage and loss moduli compared to the composite samples, which is attributed to the absence of hollow inclusions within the matrix. Among the composite formulations, increasing the filler content from 5 wt% to 15 wt% results in higher storage and loss moduli across the measured frequency range, indicating enhanced stiffness and energy dissipation with increased filler loading. To extend the accessible frequency range and better characterize the viscoelastic response, time–temperature superposition (TTS) was applied to the DMA data [105], allowing measurements at different temperatures to be shifted to an equivalent response at a chosen reference temperature:

$$E'(\omega, T) = E'(a_T \omega, T_0) \tag{5}$$

$$E''(\omega, T) = E''(a_T \omega, T_0) \tag{6}$$

where a_T is the temperature-dependent shift factor and T_0 is the reference temperature. The variation of the shift factor with temperature was described using the Williams–Landel–Ferry (WLF) relationship [106]:

$$\log\ a_T = \frac{C_1(T - T_0)}{C_2 + (T - T_0)} \tag{7}$$

where C_1 and C_2 are material-dependent constants. Using this approach, master curves were constructed at a reference temperature of 40 °C, extending the effective frequency range by approximately four orders of magnitude, as shown in Figure 18. Both storage and loss moduli

increase with increasing frequency, indicating that the composites become stiffer and exhibit greater energy dissipation at higher loading rates. The master curves also show a nonlinear dependence on frequency, reflecting the presence of multiple relaxation mechanisms active over different timescales [107]. While both composite formulations exhibit similar trends, the 15 wt% sample demonstrates a broader modulus range and stronger frequency dependence compared to the 5 wt% sample. At higher reduced frequencies, the 15 wt% composite exhibits an increase in storage modulus of approximately 30% relative to the 5 wt% sample, along with a 2–3× increase in loss modulus. This elevated loss modulus indicates enhanced energy dissipation under dynamic loading conditions, highlighting the ability to tailor viscoelastic behavior through controlled filler incorporation.

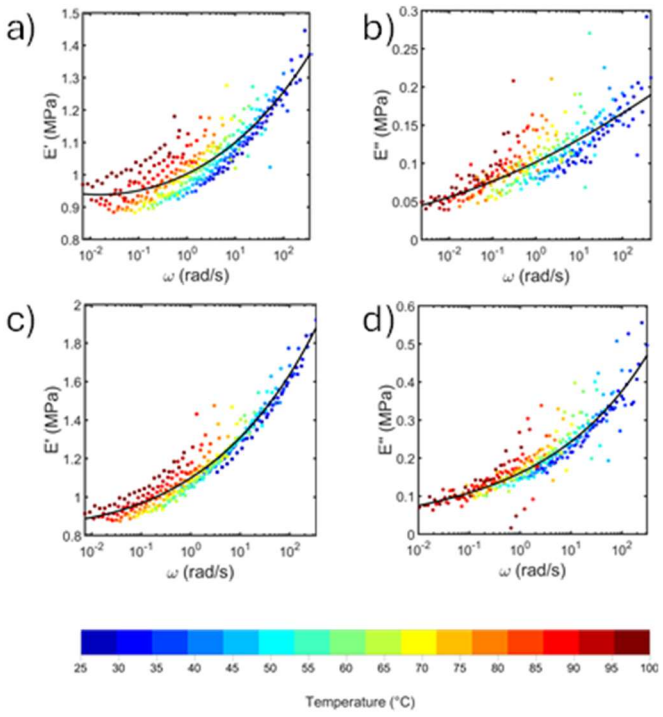


Fig. 18: Viscoelastic characterization of PDMS–HGM composites: (a) storage modulus and (b) loss modulus of 5 wt% PDMS–HGM composites obtained from DMA testing, and (c) storage modulus and (d) loss modulus of 15 wt% PDMS–HGM composites, used for TTS analysis.

5.4 Thermal Properties

Thermal characterization was conducted to evaluate the stability and heat transfer behavior of the PDMS–HGM composites as a function of filler incorporation. Understanding these properties is important for assessing material performance under elevated temperatures and dynamic operating conditions, particularly in applications where both thermal resistance and energy dissipation are relevant. The influence of PVDF-coated HGMs on degradation behavior and thermal transport was investigated using thermogravimetric and transient thermal measurements, respectively.

5.4.1 Thermal Stability

Thermal characterization was performed to evaluate both the high-temperature stability and thermal transport behavior of the composites. Thermogravimetric analysis (TGA) was used to assess thermal stability, as shown in Figure 19a, where mass loss profiles are presented for pure PDMS and composites containing 5 wt% and 15 wt% filler. All samples exhibit minimal mass loss at temperatures below approximately 400 °C, indicating stable behavior within this range. At higher temperatures, a primary degradation region is observed, corresponding to the decomposition of the PDMS matrix. Compared to pure PDMS, the composite samples show a reduced rate of mass loss and improved weight retention over the temperature range of 400–800 °C. Among the composites, the 15 wt% sample exhibits the highest residual mass at elevated temperatures, indicating enhanced thermal stability with increasing filler content. This behavior aligns with prior studies on silicone rubber–glass composites, where the incorporation of thermally stable inorganic microspheres enhances high-temperature mass retention by reducing polymer volatilization and increasing residual inorganic content [108].

5.4.2 Thermal Transport Properties

The thermal conductivity and specific heat of the composites were measured at room temperature, as shown in Figure 19b. Pure PDMS exhibited the highest thermal conductivity and specific heat among the tested samples. Incorporation of 5 wt% PVDF-coated HGMs resulted in a substantial reduction in thermal conductivity (≈70%) and specific heat (≈62%) relative to pure PDMS, consistent with the insulating nature of the hollow microspheres. Increasing the filler loading to 15 wt% led to a partial recovery in thermal transport properties, with thermal conductivity increasing by approximately 20% and specific heat increasing by nearly 90% compared to the 5 wt% composite. This trend indicates an increased contribution from the PVDF phase to heat transport within the composite, consistent with reported room-temperature thermal conductivity (≈0.18–0.26 W m^{-1} K^{-1}) and specific heat capacity (≈1.2–1.4 kJ kg^{-1} K^{-1}) of bulk PVDF [109]. At higher filler loadings, reduced particle spacing and improved connectivity between coated microspheres likely promote the formation of more effective thermal pathways, where closer particle proximity facilitates capillary bridge formation between adjacent PVDF-coated HGMs and results in a more continuous conductive network. Overall, these results demonstrate that thermal transport properties can be tuned through filler loading, balancing the insulating effect of hollow microspheres at low concentrations with enhanced heat conduction at higher loadings due to increased PVDF network connectivity.

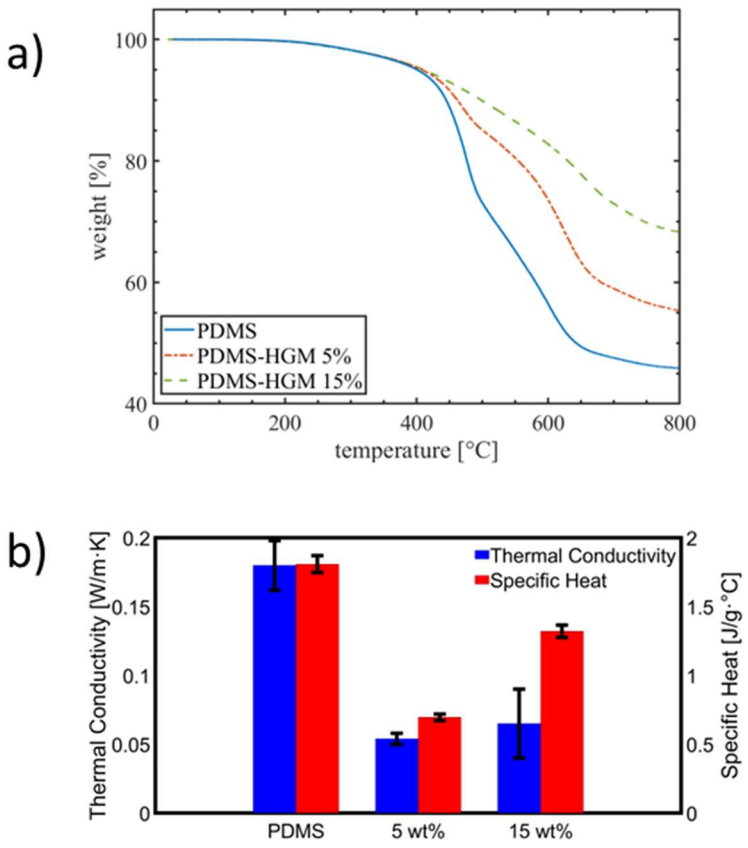


Fig. 19: Thermal characterization of PDMS–HGM composites: (a) TGA results for pure PDMS and PDMS–HGM composites at 5 wt% and 15 wt%, and (b) thermal conductivity and specific heat of PDMS, 5 wt%, and 15 wt% PDMS–HGM composites.

5.5 Dynamic Testing

To demonstrate the piezoelectric response of PDMS–HGM composites under dynamic loading, both drop tests and blast tests were performed. These experiments were used to evaluate the electrical response of the composite under controlled impact conditions as well as under high-intensity pressure loading.

5.5.1 Drop Impact Testing

In drop tests, a Squirtle model (modified based on an open-source model by Yuxiu YUX from the Bambu Lab online model library) was fabricated using PLA via fused deposition modeling, and the PDMS–HGM (15 wt%) composite was subsequently deposited onto the top shell using direct ink writing. A golf ball (45.6 g) was released from controlled heights of 15, 20, and 30 cm (Fig. 20a–b), and a clear voltage signal was measured for each impact event (Fig. 20c). The peak voltage increased with increasing drop height, indicating a direct relationship between impact conditions and the measured electrical response.

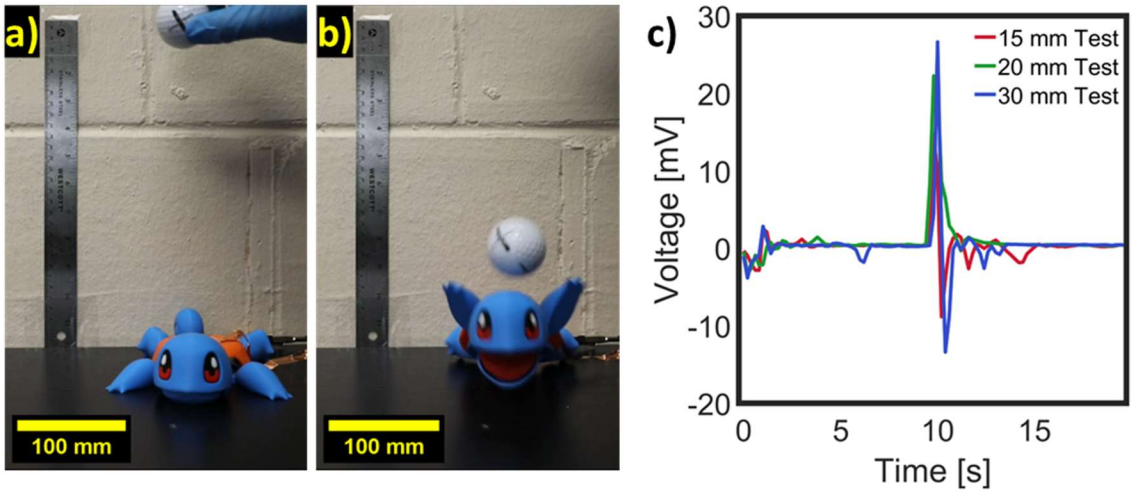


Fig. 20: Demonstrations of the piezoelectric responses of PVDF-HGM composites under dynamic loading. The drop tests (a) prior to release and (b) at the moment of impact of the weight onto the PVDF-HGM composites coated surface, and (c) the resulting voltage output demonstrating piezoelectric responses.

5.5.2 Blast Loading Response

To assess the response of the composite under more extreme conditions, blast tests were conducted using a compressed gas-driven setup. A PDMS–HGM film was printed onto a commercial foam

earplug, as shown in Figure 21a, and subsequently inserted into an artificial human ear mounted within a head block placed inside the blast chamber (Figure 21b). During testing, blast overpressure waves with peak amplitudes approaching 90 kPa were generated, producing a characteristic Friedlander-type waveform with a sharp rise in pressure followed by an exponential decay, as shown in Figure 21c [110]. The voltage signal measured from the composite-coated earplug exhibited a synchronized electrical response during the blast event (Figure 21d), confirming that the material can transduce high-rate mechanical loading into an electrical signal. These results highlight the potential of the composite for integration into wearable hearing protective devices, where both mechanical compliance and dynamic sensing capability are required under transient loading conditions [110].

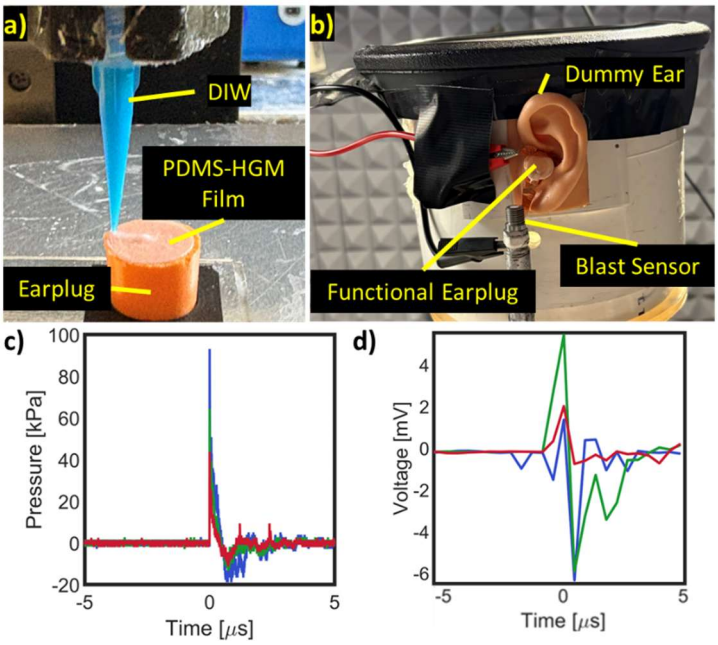


Fig. 21: Blast test demonstration of piezoelectric response in PVDF–HGM composites. (a) 3D printing of the PDMS–HGM composite film onto an earplug, (b) insertion of the composite-coated earplug into a dummy ear and head block for blast testing, (c) measured blast wave profile during testing, and (d) corresponding voltage output generated by the PVDF–HGM composite.

Chapter 6: Computational Modeling and Potential Biomedical Applications

6.1 Introduction

The developed PVDF-coated HGM composites exhibit tunable mechanical, thermal, and electromechanical behavior as a function of filler loading and processing through DIW. Building on these established structure–property relationships, the work is extended toward computational modeling and functional applications. Preliminary finite element simulations were conducted to examine stress distribution and particle–particle interactions within the composite, providing insight into the formation of load transfer pathways and network behavior. In parallel, a proof-of-concept bioinspired sensing system was developed by leveraging the flexibility and electromechanical response of DIW-fabricated structures. A buckling PDMS architecture was combined with conductive and piezoelectric coatings to enable signal generation under flow-induced dynamic loading conditions. These results highlight the potential of the composite system for multifunctional applications while offering initial modeling-based insight into the mechanisms governing its behavior.

6.2 Computational Modeling of Microstructure and Network Behavior

6.2.1 Modeling Approach

Finite element simulations were conducted in ABAQUS to qualitatively replicate the percolating network behavior observed experimentally and to better understand particle–particle interactions within the composite. Microscopy observations, as shown in Figure 22a, revealed adjacent PVDF-coated HGMs forming interconnected regions through localized bridging, which motivated the

development of a simplified computational representation. Based on this observation, a two-dimensional model was constructed in ABAQUS to capture the essential features of this behavior, as illustrated in Figure 22b. The model consisted of two neighboring coated microspheres positioned in close proximity and connected through a PVDF bridge to mimic the experimentally observed network formation. These coated HGMs were embedded within a square PDMS matrix to approximate a representative region corresponding to a 15 wt% HGM loading, with the equivalent volume fraction determined through back-calculation. Geometric and material parameters were defined using experimentally measured and literature-supported values, where the HGMs were modeled with an average diameter of 47.8 ± 1.33 μm and a shell thickness of 160 ± 99.7 nm, while the PVDF coating thickness was taken as 481 ± 252 nm as determined earlier. The PDMS matrix was modeled using a hyperelastic constitutive formulation to capture its nonlinear mechanical response, while the coated HGMs were treated as composite inclusions. This modeling approach was intended to capture the key features of particle interaction and network formation observed experimentally, rather than to provide a fully predictive representation of the composite behavior.

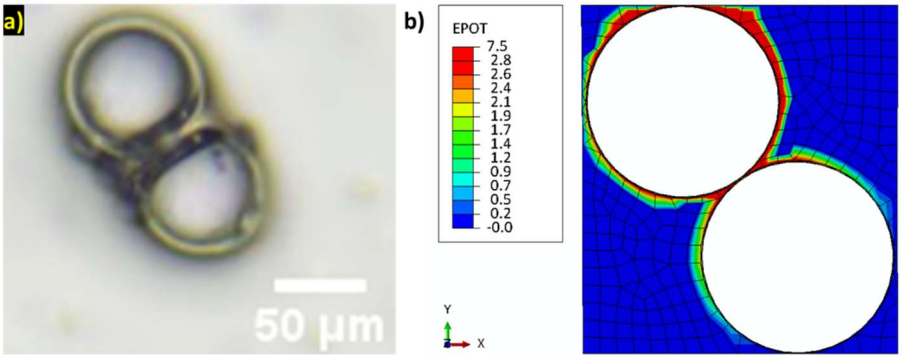


Fig. 22: (a) Microscopy image of adjacent PVDF-coated HGMs exhibiting interparticle bridging. (b) Corresponding two-dimensional finite element model developed in ABAQUS to represent particle interaction and percolation within the PDMS matrix.

6.2.2 Network Formation and Percolation Behavior

The simplified finite element model shown in Figure 22b provides a qualitative representation of network formation and percolation behavior between adjacent PVDF-coated HGMs within the PDMS matrix. The modeled configuration captures the experimentally observed interparticle bridging by representing neighboring coated particles connected through a compliant PVDF region, enabling the evaluation of localized particle–particle interactions within the surrounding matrix. The presence of the PVDF bridge provides a continuous link between adjacent HGMs, illustrating how localized interactions can form interconnected regions within the composite. This simplified configuration qualitatively demonstrates how reduced interparticle spacing may facilitate the development of network-like structures. Although the current simulation results remain preliminary and do not fully capture the complexity of the composite microstructure, the model reproduces the general concept of percolating network formation observed experimentally. The PDMS matrix was also assigned hyperelastic material behavior, allowing deformation of the surrounding matrix to be represented more realistically than with a purely linear elastic approximation. While further refinement is needed to improve geometric fidelity, material representation, and predictive capability, the present model establishes a useful foundation for examining how these interconnected structures contribute to the development of load transfer pathways within the composite, which is further explored through the simulation results in the following section.

6.2.3 Stress Distribution and Electromechanical Response

The stress distribution, deformation behavior, and voltage output obtained from the finite element model provide insight into the role of particle interaction in facilitating load transfer and electromechanical response within the composite. Representative results are shown in Figure 23,

where the von Mises stress distribution, displacement magnitude, and voltage output are presented for the simplified two-particle configuration. The stress contours reveal localized stress concentrations in the regions surrounding the HGMs, with elevated stresses observed near the particle interfaces and within the interparticle bridge, suggesting that mechanical interaction between adjacent particles influences how load is distributed through the surrounding PDMS matrix. In particular, the presence of the PVDF bridge promotes a more continuous stress transfer between neighboring inclusions compared to isolated particles, indicating that interconnected structures may contribute to more efficient load distribution within the composite. The displacement field further supports this behavior by showing deformation of the PDMS matrix around the inclusions and through the interparticle region, highlighting the role of the compliant matrix in mediating interactions between particles. In addition to the mechanical response, the voltage output distribution illustrates regions of potential generation associated with deformation of the PVDF-coated HGMs, with elevated values observed near particle interfaces and within the interparticle region, suggesting that localized deformation and particle interaction may contribute to enhanced electromechanical response. Although the absolute magnitudes predicted by the model are not intended to be quantitatively accurate, the results qualitatively demonstrate how particle interaction and network formation can influence both stress transfer and voltage generation within the composite. This behavior is consistent with experimental observations, where composites containing PVDF-coated HGMs exhibited enhanced mechanical response and improved electromechanical performance compared to the PDMS matrix alone, supporting the hypothesis that interconnected particle structures play a key role in governing the coupled mechanical and piezoelectric behavior of the system.

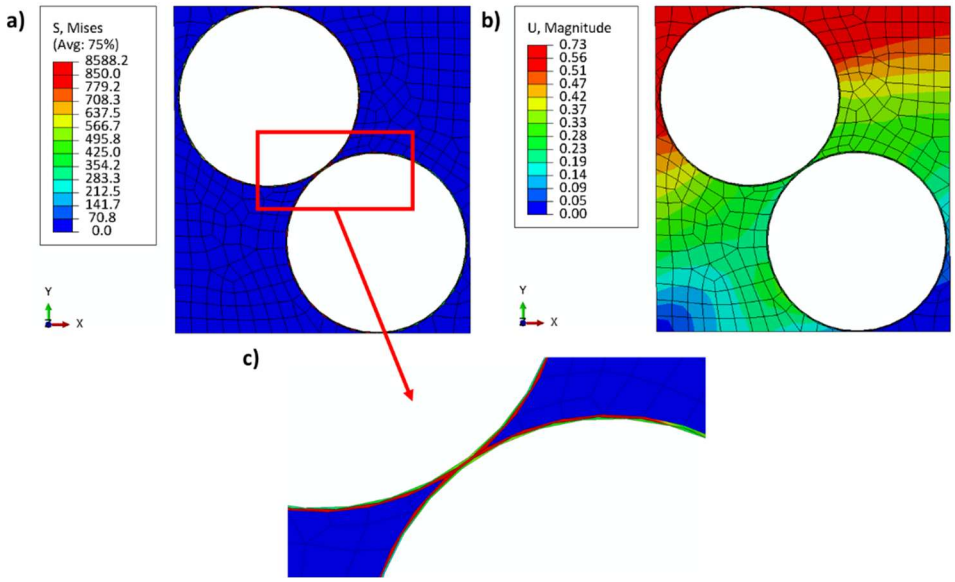


Fig. 23: (a) von Mises stress distribution and (b) displacement magnitude for the simplified two-particle model embedded in a PDMS matrix , and (c) zoomed-in view highlighting interfacial stress concentration in the narrow matrix ligament between adjacent inclusions.

6.2.4 Discussion and Future Directions in Modeling

While the present modeling approach provides a useful qualitative framework for understanding particle interaction and network formation, several improvements are necessary to enhance its predictive capability. One key limitation is the absence of fully coupled electromechanical modeling, as the current simulations primarily capture mechanical behavior without explicitly resolving the piezoelectric response of the PVDF phase. Incorporating multiphysics coupling would enable direct simulation of voltage generation and provide a more complete understanding of the relationship between mechanical deformation and electrical output. Additionally, the simplified two-particle geometry does not fully represent the complexity of the composite microstructure, and future work should consider more realistic representative volume elements (RVEs) that include multiple particles and statistically relevant spatial distributions. Extending the

model to evaluate different filler contents would also be important for capturing how variations in particle concentration influence interparticle spacing, network formation, and overall composite behavior. Furthermore, improved representation of the PVDF coating and particle–matrix interface, including interfacial properties and potential debonding effects, would allow for more accurate modeling of load transfer mechanisms. These developments would enable a more robust modeling framework capable of linking microstructural features to the mechanical and electromechanical performance of the composite system.

6.3 Bioinspired Electromechanical Sensing Application

6.3.1 Fabrication of Buckling Structure

The buckling structure was designed based on a bifurcation-inspired geometry, where the ratio of key geometric parameters (w/L) was selected to achieve controlled structural instability under loading. This design approach was adapted from a two-dimensional bifurcation model to enable predictable buckling behavior. A parameterized design framework was developed using a Python script, allowing systematic variation of geometric features and automated generation of G-code for DIW fabrication. Using this approach, multiple samples were produced with varying dome height, wall thickness, brim size, and nozzle diameter to evaluate their influence on the buckling response, although optimization of these parameters is still ongoing. The structures were fabricated using DIW to produce compliant PDMS architectures, as shown in Figure 24a, and after curing, the printed structures exhibited consistent geometries across a range of sizes and design parameters (Figure 24b). A thin gold layer was then deposited on the inner surface via sputter coating to serve as a conductive electrode while maintaining conformity with the flexible substrate (Figure 24c). Following electrode integration, a PVDF coating was applied to introduce piezoelectric functionality. Two identical buckling structures were subsequently assembled and bonded using a

silicone adhesive to form a sealed configuration, taking advantage of the inherent compatibility between silicone and PDMS for robust interfacial adhesion. The assembled structures, shown in Figure 24d, demonstrate integration into a confined geometry suitable for flow-based evaluation. This fabrication strategy combines parametric design, additive manufacturing, and post-processing to produce a functional soft structure, where DIW enables scalable fabrication of tunable geometries and the integration of conductive and piezoelectric layers provides a simple and adaptable pathway for developing electromechanical systems.

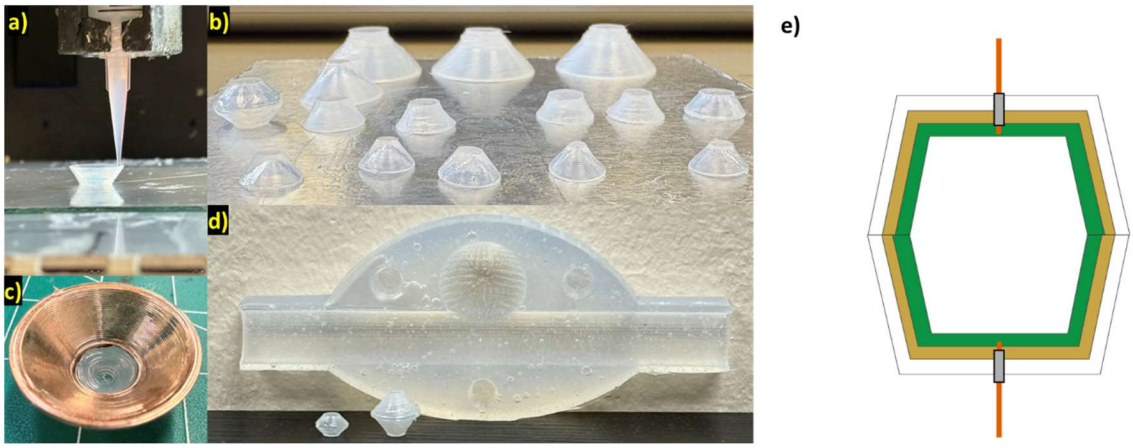


Fig. 24: (a) DIW printing of PDMS buckling structure, (b) fabricated structures with varying geometries, (c) inner surface after gold sputter coating, and (d) assembled PDMS structure integrated within an artery- mimicking, and (e) schematic of the assembled buckling structure with top and bottom electrodes.

6.3.2 Simulated Arterial Flow Setup

To evaluate the response of the fabricated buckling structure under dynamic flow conditions, a simplified flow system was developed using a closed-loop setup driven by a Kamoer UIP pump (Kamoer, Shenzhen, China). The pump enabled controlled, cyclic fluid flow through flexible tubing, providing a repeatable method for simulating pulsatile conditions. The assembled PDMS

buckling structure was placed within the flow path and integrated into a confined geometry, allowing it to experience flow-induced pressure fluctuations and mechanical deformation during operation. The corresponding device configuration is shown in Figure 24e, where the structure is positioned to deform under cyclic loading while incorporating top and bottom electrodes for electrical signal generation. Under these conditions, fluid flow induces periodic deformation of the compliant structure, resulting in a coupled mechanical and electrical response. This setup was designed as a proof-of-concept platform to investigate how flow-induced deformation of a soft, structured system can generate measurable electrical signals. While the physical representation of the system is simplified, it provides a controlled environment for evaluating the interaction between fluid flow, structural deformation, and electromechanical response, serving as a foundation for potential applications in sensing or actuation within soft and bioinspired systems.

6.3.3 Electromechanical Response

The electromechanical response of the buckling structure under cyclic flow conditions was evaluated by measuring the voltage output generated during operation. Representative voltage–time data are shown in Figure 25a, where transient voltage peaks correspond to deformation of the structure induced by pulsatile fluid flow. As indicated by the pulse initiation marker in Figure 25a, the electrical response occurs immediately following the onset of the flow pulse, demonstrating temporal correspondence between the applied mechanical input and measured voltage signal. The presence of repeatable peaks indicates that deformation of the compliant PDMS structure, coupled with the PVDF layer, produces a detectable electrical response under dynamic loading conditions. In addition to transient voltage generation, the ability of the system to retain charge was qualitatively assessed using a bridge-circuit measurement incorporating a storage capacitor (0.1 μF), as shown in Figure 25b. In this configuration, the generated signal was routed through the

bridge circuit to the capacitor, enabling accumulation of charge produced during successive flow pulses. The inset in Figure 25b further highlights the step-like accumulation behavior, where discrete charge increments are observed following successive pulses. The results exhibit a step-like charge response following each fluid pulse, with incremental increases in accumulated charge magnitude over time. This behavior indicates that the generated signal can be captured and accumulated over successive flow cycles, providing further evidence of functional electromechanical coupling within the system. Although the magnitude of the generated signal is not optimized and may be influenced by factors such as coating uniformity, electrode configuration, and structural variability, the results demonstrate a repeatable and measurable electrical response driven by flow-induced deformation. These findings support the feasibility of using such structures as soft, deformation-driven signal generators and establish a foundation for further refinement and optimization.

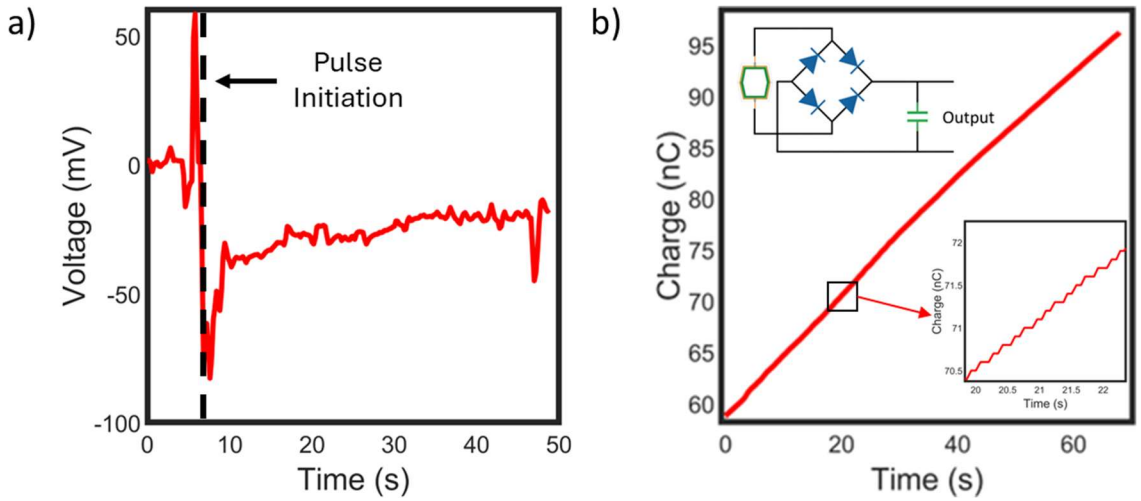


Fig. 25: (a) Voltage output as a function of time under pulsatile fluid flow, showing transient response behavior and pulse initiation, and (b) bridge-circuit measurement showing stepwise charge accumulation over time, with inset highlighting discrete charge increments.

6.3.4 Discussion and Application Outlook

The results presented in this section demonstrate a proof-of-concept system in which a soft, DIW-fabricated buckling structure generates a measurable electrical response under deformation. While the current implementation is not optimized, the observed behavior establishes a direct link between structural design, mechanical deformation, and voltage output, highlighting the potential of these systems as deformation-driven electromechanical devices. From an application perspective, this approach is relevant for pressure sensing and flow monitoring in soft or confined environments, where structural deformation can serve as a transduction mechanism. In particular, such structures may be applicable to geometries resembling vascular features, where localized deformation and fluid–structure interactions are present. In these environments, the generation of localized electrical signals may influence charge distributions within the surrounding medium, providing a pathway for interactions with suspended particles under dynamic conditions. However, these effects remain conceptual and require further investigation. Several limitations are present in the current system. Variability in PVDF coating thickness and uniformity may affect the consistency of the electromechanical response, while the electrode configuration and assembly process introduce additional sources of variability in signal generation. Furthermore, the magnitude of the generated voltage remains relatively low and has not been optimized for specific applications. Future work should focus on improving fabrication control to achieve more uniform coatings and consistent structural geometries, as well as refining electrode integration to enhance signal stability. Integration with external electronics for signal amplification and processing will also be critical for advancing the system toward practical applications. Overall, this work establishes a foundation for the development of soft, structure-driven electromechanical systems with potential for sensing and actuation in complex environments.

6.4 Summary

This work demonstrated how the developed PVDF-coated HGM composite system can be extended from material characterization to functional applications. Computational modeling provided qualitative insight into particle interactions and network formation, supporting experimentally observed structure–property relationships. A proof-of-concept electromechanical system was then developed using DIW-fabricated buckling structures, which generated a measurable voltage output under flow-induced deformation. These results highlight the potential of combining tailored microstructures with soft architectures to achieve tunable electromechanical functionality. Overall, this work reinforces the connection between processing, structure, and properties, and demonstrates a pathway toward integrating these materials into application-driven systems.

Chapter 7: Conclusions

This work presented the development of lightweight, multifunctional PDMS-based composites incorporating PVDF-coated hollow glass microspheres, with a focus on establishing clear processing–structure–property–application relationships. A scalable fabrication approach was developed by coating HGMs with PVDF using a solution-based method, followed by integration into a PDMS matrix and processing via DIW. This enabled the creation of tunable composite systems with controlled microstructure and geometry. Microstructural analysis confirmed uniform PVDF coating and the formation of particle–particle interactions through localized bridging, which contributed to network-like behavior within the composite. Mechanical testing demonstrated that while stiffness decreased with increasing filler content, the composites exhibited enhanced specific energy absorption, indicating improved energy dissipation capabilities at reduced density. Electromechanical testing further revealed that the incorporation of PVDF-coated HGMs significantly enhanced voltage output compared to the PDMS baseline, with optimal performance observed at intermediate filler loadings due to a balance between particle connectivity and matrix compliance. Thermal characterization showed that the composites maintained stability at elevated temperatures and exhibited tunable thermal transport behavior depending on filler content. Rheological analysis confirmed shear-thinning behavior suitable for direct ink writing, while also suggesting that processing-induced shear may contribute to dipole alignment within the PVDF phase. Preliminary computational modeling provided qualitative insight into particle interaction and network formation, supporting experimental observations of load transfer pathways and electromechanical response. Building on these findings, a proof-of-concept soft electromechanical system was developed using DIW-fabricated buckling structures, demonstrating measurable voltage output under flow-induced deformation. This highlights the potential for integrating these

materials into functional systems. Overall, this study demonstrates that PVDF-coated HGM composites offer a versatile platform for lightweight, tunable, and functional materials. By linking processing methods to microstructural features and resulting properties, this work establishes a foundation for future development of soft electromechanical systems for sensing and related applications.

References

[1] L. Yan, H. Xu, Lightweight composite materials in automotive engineering: State-of-the-art and future trends, Alexandria Engineering Journal 118 (2025) 1–10. https://doi.org/10.1016/j.aej.2024.12.002.

[2] Jobanpreet Singh, K. Srivastawa, S. Jana, C. Dixit, R. S, Advancements in Lightweight Materials for Aerospace Structures: A Comprehensive Review, AAJ 2 (2024) 173–183. https://doi.org/10.61359/11.2106-2409.

[3] J. Qin, Y. Tang, Y. Zeng, X. Liu, D. Tang, Recent advances in flexible sensors: From sensing materials to detection modes, TrAC Trends in Analytical Chemistry 181 (2024) 118027. https://doi.org/10.1016/j.trac.2024.118027.

[4] B. Zazoum, K.M. Batoo, M.A.A. Khan, Recent Advances in Flexible Sensors and Their Applications, Sensors 22 (2022) 4653. https://doi.org/10.3390/s22124653.

[5] S. Yin, D.R. Yao, Y. Song, W. Heng, X. Ma, H. Han, W. Gao, Wearable and Implantable Soft Robots, Chem. Rev. 124 (2024) 11585–11636. https://doi.org/10.1021/acs.chemrev.4c00513.

[6] A. Dinesh, S. Indhumathi, M. Pichumani, Self-sensing cement composites for structural health monitoring: From know-how to do-how, Automation in Construction 160 (2024) 105304. https://doi.org/10.1016/j.autcon.2024.105304.

[7] Y. Tao, R. Zhang, X. Hu, Y. Ou, M. Ren, J. Sun, H. Zhang, T. Peijs, A comprehensive review on fiber-based self-sensing polymer composites for in situ structural health monitoring, Adv Compos Hybrid Mater 8 (2025) 339. https://doi.org/10.1007/s42114-025-01413-y.

[8] S. Li, J. Zhang, J. He, W. Liu, Y. Wang, Z. Huang, H. Pang, Y. Chen, Functional PDMS Elastomers: Bulk Composites, Surface Engineering, and Precision Fabrication, Advanced Science 10 (2023) 2304506. https://doi.org/10.1002/advs.202304506.

[9] M. Tajik HesarAmiri, P. Khattami Kermanshahi, R. Bagherzadeh, M. Yousefzadeh, P. Fakhri, A multilayer piezoelectric nanogenerator based on PVDF and $BaTiO_3$ nanocomposite with enhanced performance induced by simultaneously electrospinning and electrospraying, Journal of Industrial Textiles 54 (2024) 15280837241302259. https://doi.org/10.1177/15280837241302259.

[10] K. Uchino, Piezoelectric actuators and ultrasonic motors, Nachdr., Kluwer, Boston, 2000.

[11] R. Dallaev, T. Pisarenko, D. Sobola, F. Orudzhev, S. Ramazanov, T. Trčka, Brief Review of PVDF Properties and Applications Potential, Polymers 14 (2022) 4793. https://doi.org/10.3390/polym14224793.

[12] D. Kim, J.A. Rogers, Stretchable Electronics: Materials Strategies and Devices, Advanced Materials 20 (2008) 4887–4892. https://doi.org/10.1002/adma.200801788.

[13] S. Hu, Z. Shi, W. Zhao, L. Wang, G. Yang, Multifunctional piezoelectric elastomer composites for smart biomedical or wearable electronics, Composites Part B: Engineering 160 (2019) 595–604. https://doi.org/10.1016/j.compositesb.2018.12.077.

[14] C. Dagdeviren, B.D. Yang, Y. Su, P.L. Tran, P. Joe, E. Anderson, J. Xia, V. Doraiswamy, B. Dehdashti, X. Feng, B. Lu, R. Poston, Z. Khalpey, R. Ghaffari, Y. Huang, M.J. Slepian, J.A. Rogers, Conformal piezoelectric energy harvesting and storage from motions of the heart, lung, and diaphragm, Proc. Natl. Acad. Sci. U.S.A. 111 (2014) 1927–1932. https://doi.org/10.1073/pnas.1317233111.

[15] H. Yuan, T. Lei, Y. Qin, R. Yang, Flexible electronic skins based on piezoelectric nanogenerators and piezotronics, Nano Energy 59 (2019) 84–90. https://doi.org/10.1016/j.nanoen.2019.01.072.

[16] A. Jain, P. K. J., A.Kr. Sharma, A. Jain, R. P.N, Dielectric and piezoelectric properties of PVDF/PZT composites: A review, Polymer Engineering & Sci 55 (2015) 1589–1616. https://doi.org/10.1002/pen.24088.

[17] H. Kim, T. Fernando, M. Li, Y. Lin, T.-L.B. Tseng, Fabrication and characterization of 3D printed $BaTiO_3$ /PVDF nanocomposites, Journal of Composite Materials 52 (2018) 197–206. https://doi.org/10.1177/0021998317704709.

[18] C.R. Bowen, H.A. Kim, P.M. Weaver, S. Dunn, Piezoelectric and ferroelectric materials and structures for energy harvesting applications, Energy Environ. Sci. 7 (2014) 25–44. https://doi.org/10.1039/C3EE42454E.

[19] Z.S. Radeef, A.-R.K. Jweri, A.M. Alsayah, M.J. Alshukri, M. Khaled, Advances in piezoelectric energy harvesting: Materials, configurations, and power optimisation strategies, Results in Engineering 28 (2025) 107782. https://doi.org/10.1016/j.rineng.2025.107782.

[20] J. Rödel, W. Jo, K.T.P. Seifert, E. Anton, T. Granzow, D. Damjanovic, Perspective on the Development of Lead-free Piezoceramics, Journal of the American Ceramic Society 92 (2009) 1153–1177. https://doi.org/10.1111/j.1551-2916.2009.03061.x.

[21] G. Magdy, A.H. Hassanin, I. Kandas, N. Shehata, PVDF nanostructures characterizations and techniques for enhanced piezoelectric response: A review, Materials Chemistry and Physics 325 (2024) 129760. https://doi.org/10.1016/j.matchemphys.2024.129760.

[22] N. Ahbab, S. Naz, T.-B. Xu, S. Zhang, A Comprehensive Review of Piezoelectric PVDF Polymer Fabrications and Characteristics, Micromachines 16 (2025) 386. https://doi.org/10.3390/mi16040386.

[23] F. Memarian, R. Mohammadi, R. Akrami, M. Bodaghi, M. Fotouhi, A Comprehensive Review of Nanocomposite PVDF as a Piezoelectric Material: Evaluating Manufacturing

Methods, Energy Efficiency and Performance, Nanofab 8 (2023). https://doi.org/10.37819/nanofab.8.1775.

[24] Y. Wu, Y. Ma, H. Zheng, S. Ramakrishna, Piezoelectric materials for flexible and wearable electronics: A review, Materials & Design 211 (2021) 110164. https://doi.org/10.1016/j.matdes.2021.110164.

[25] S. Lanceros-Méndez, C.M. Costa, eds., Piezoelectric Polymers and Polymer Composites for Advanced Applications, Springer Nature Switzerland, Cham, 2025. https://doi.org/10.1007/978-3-031-88736-9.

[26] R. Ariati, F. Sales, A. Souza, R.A. Lima, J. Ribeiro, Polydimethylsiloxane Composites Characterization and Its Applications: A Review, Polymers 13 (2021) 4258. https://doi.org/10.3390/polym13234258.

[27] T. Raman Venkatesan, A.A.-L. Hausmann, J.E.Q. Quinsaat, A. Neels, D.M. Opris, Ferroelectric elastomers of functionalized polar fillers in polydimethylsiloxane with improved dielectric and ferroelectric properties, Composites Part B: Engineering 293 (2025) 112076. https://doi.org/10.1016/j.compositesb.2024.112076.

[28] A.Z. Romli, N.S. Zahari, N.A.D. Sapari, M.M. Mohd Ghaztar, N.N.I. Nik Ibrahim, EFFECT OF POLYVINYLIDENE FLUORIDE LOADINGS ON THE MECHANICAL PROPERTIES AND BURNING RATE OF EPOXY COMPOSITES, J. Teknol. 87 (2025) 839–846. https://doi.org/10.11113/jurnalteknologi.v87.20198.

[29] D.F. Tassaw, M. Barburski, B.B. Kassie, The Role of Hollow Glass Microspheres as Functional Fillers in Fiber-Reinforced Polymer Composites: A Review, Materials 18 (2025) 4974. https://doi.org/10.3390/ma18214974.

[30] A. Aruniit, J. Kers, J. Majak, A. Krumme, K. Tall, Influence of hollow glass microspheres on the mechanical and physical properties and cost of particle reinforced polymer composites; pp. 160–165, PEAS 61 (2012) 160–165. https://doi.org/10.3176/proc.2012.3.03.

[31] O.A. Afolabi, K. Kanny, T.P. Mohan, Analysis of Particle Variation Effect on Flexural Properties of Hollow Glass Microsphere Filled Epoxy Matrix Syntactic Foam Composites, Polymers 14 (2022) 4848. https://doi.org/10.3390/polym14224848.

[32] Y. Feng, W.L. Li, J.P. Wang, J.H. Yin, W.D. Fei, Core–shell structured $BaTiO_3$ @carbon hybrid particles for polymer composites with enhanced dielectric performance, J. Mater. Chem. A 3 (2015) 20313–20321. https://doi.org/10.1039/C5TA04777C.

[33] Y. Jiang, A.X. Serrano, W. Choi, R.C. Advincula, H.F. Wu, Advanced and functional composite materials via additive manufacturing: Trends and perspectives, MRS Communications 14 (2024) 449–459. https://doi.org/10.1557/s43579-024-00625-5.

[34] M.A.S.R. Saadi, A. Maguire, N.T. Pottackal, M.S.H. Thakur, M.Md. Ikram, A.J. Hart, P.M. Ajayan, M.M. Rahman, Direct Ink Writing: A 3D Printing Technology for Diverse Materials, Advanced Materials 34 (2022) 2108855. https://doi.org/10.1002/adma.202108855.

[35] S. Tagliaferri, A. Panagiotopoulos, C. Mattevi, Direct ink writing of energy materials, Mater. Adv. 2 (2021) 540–563. https://doi.org/10.1039/D0MA00753F.

[36] C. Li, C. Feng, L. Zhang, L. Zhang, L. Wang, Direct ink writing of polymer-based materials—A review, Polymer Engineering & Sci 65 (2025) 431–454. https://doi.org/10.1002/pen.27038.

[37] T. Ma, Y. Zhang, K. Ruan, H. Guo, M. He, X. Shi, Y. Guo, J. Kong, J. Gu, Advances in 3D printing for polymer composites: A review, InfoMat 6 (2024) e12568. https://doi.org/10.1002/inf2.12568.

[38] S.D. Mahapatra, P.C. Mohapatra, A.I. Aria, G. Christie, Y.K. Mishra, S. Hofmann, V.K. Thakur, Piezoelectric Materials for Energy Harvesting and Sensing Applications: Roadmap for Future Smart Materials, Advanced Science 8 (2021) 2100864. https://doi.org/10.1002/advs.202100864.

[39] S. Mohith, A.R. Upadhya, K.P. Navin, S.M. Kulkarni, M. Rao, Recent trends in piezoelectric actuators for precision motion and their applications: a review, Smart Mater. Struct. 30 (2021) 013002. https://doi.org/10.1088/1361-665X/abc6b9.

[40] V. Bouad, M. Girardot, V. Ladmiral, S. Barrau, Piezoelectric fluorinated polymer composites: A review on coupling agents at the filler/matrix interface, Polymer Composites 45 (2024) 3861–3882. https://doi.org/10.1002/pc.28064.

[41] M. Habib, I. Lantgios, K. Hornbostel, A review of ceramic, polymer and composite piezoelectric materials, J. Phys. D: Appl. Phys. 55 (2022) 423002. https://doi.org/10.1088/1361-6463/ac8687.

[42] Y. Yan, L.D. Geng, H. Liu, H. Leng, X. Li, Y.U. Wang, S. Priya, Near-ideal electromechanical coupling in textured piezoelectric ceramics, Nat Commun 13 (2022) 3565. https://doi.org/10.1038/s41467-022-31165-y.

[43] S. Mirjalali, A. Mahdavi Varposhti, S. Abrishami, R. Bagherzadeh, M. Asadnia, S. Huang, S. Peng, C. Wang, S. Wu, A Review on Wearable Electrospun Polymeric Piezoelectric Sensors and Energy Harvesters, Macro Materials & Eng 308 (2023) 2200442. https://doi.org/10.1002/mame.202200442.

[44] Y. Chen, Y. Yang, M. Li, E. Chen, W. Mu, R. Fisher, R. Yin, Wearable Actuators: An Overview, Textiles 1 (2021) 283–321. https://doi.org/10.3390/textiles1020015.

[45] S. Mishra, L. Unnikrishnan, S.K. Nayak, S. Mohanty, Advances in Piezoelectric Polymer Composites for Energy Harvesting Applications: A Systematic Review, Macro Materials & Eng 304 (2019) 1800463. https://doi.org/10.1002/mame.201800463.

[46] M. Abbasipour, R. Khajavi, A.H. Akbarzadeh, A Comprehensive Review on Piezoelectric Polymeric and Ceramic Nanogenerators, Adv Eng Mater 24 (2022) 2101312. https://doi.org/10.1002/adem.202101312.

[47] P. Martins, A.C. Lopes, S. Lanceros-Mendez, Electroactive phases of poly(vinylidene fluoride): Determination, processing and applications, Progress in Polymer Science 39 (2014) 683–706. https://doi.org/10.1016/j.progpolymsci.2013.07.006.

[48] S. Mohammadpourfazeli, S. Arash, A. Ansari, S. Yang, K. Mallick, R. Bagherzadeh, Future prospects and recent developments of polyvinylidene fluoride (PVDF) piezoelectric polymer; fabrication methods, structure, and electro-mechanical properties, RSC Adv. 13 (2023) 370–387. https://doi.org/10.1039/D2RA06774A.

[49] A. Safari, E.K. Akdoğan, eds., Piezoelectric and Acoustic Materials for Transducer Applications, Springer US, Boston, MA, 2008. https://doi.org/10.1007/978-0-387-76540-2.

[50] H. Jin, X. Gao, K. Ren, J. Liu, L. Qiao, M. Liu, W. Chen, Y. He, S. Dong, Z. Xu, F. Li, Review on Piezoelectric Actuators Based on High-Performance Piezoelectric Materials, IEEE Trans. Ultrason., Ferroelect., Freq. Contr. 69 (2022) 3057–3069. https://doi.org/10.1109/TUFFC.2022.3175853.

[51] H. Kabra, H.A. Deore, P. Patil, Review on advanced piezoelectric materials ($BaTiO_3$, PZT), Journal of Emerging Technologies and Innovative Research 9 (2019) 950–957.

[52] S.J. Rupitsch, Piezoelectric Sensors and Actuators: Fundamentals and Applications, Springer Berlin Heidelberg, Berlin, Heidelberg, 2019. https://doi.org/10.1007/978-3-662-57534-5.

[53] S.A. Pullano, C.D. Critello, M.G. Bianco, M. Menniti, A.S. Fiorillo, PVDF Ultrasonic Sensors for In-Air Applications: A Review, IEEE Trans. Ultrason., Ferroelect., Freq. Contr. 68 (2021) 2324–2335. https://doi.org/10.1109/TUFFC.2021.3078069.

[54] X. Zhou, K. Zhou, D. Zhang, C. Bowen, Q. Wang, J. Zhong, Y. Zhang, Perspective on Porous Piezoelectric Ceramics to Control Internal Stress, Nanoenergy Advances 2 (2022) 269–290. https://doi.org/10.3390/nanoenergyadv2040014.

[55] S. Bauer, F. Bauer, Piezoelectric Polymers and Their Applications, in: Piezoelectricity, Springer Berlin Heidelberg, Berlin, Heidelberg, 2008: pp. 157–177. https://doi.org/10.1007/978-3-540-68683-5_6.

[56] Z.-X. Huang, L.-W. Li, Y.-Z. Huang, W.-X. Rao, H.-W. Jiang, J. Wang, H.-H. Zhang, H.-Z. He, J.-P. Qu, Self-poled piezoelectric polymer composites via melt-state energy implantation, Nat Commun 15 (2024) 819. https://doi.org/10.1038/s41467-024-45184-4.

[57] X. Xu, Y. Chen, P. He, S. Wang, K. Ling, L. Liu, P. Lei, X. Huang, H. Zhao, J. Cao, J. Yang, Wearable CNT/Ti3C2Tx MXene/PDMS composite strain sensor with enhanced stability for real-time human healthcare monitoring, Nano Res. 14 (2021) 2875–2883. https://doi.org/10.1007/s12274-021-3536-3.

[58] M. Amjadi, K. Kyung, I. Park, M. Sitti, Stretchable, Skin-Mountable, and Wearable Strain Sensors and Their Potential Applications: A Review, Adv Funct Materials 26 (2016) 1678–1698. https://doi.org/10.1002/adfm.201504755.

[59] H. Wu, F. Zhuo, H. Qiao, L. Kodumudi Venkataraman, M. Zheng, S. Wang, H. Huang, B. Li, X. Mao, Q. Zhang, Polymer-/Ceramic-based Dielectric Composites for Energy Storage and Conversion, Energy & Environ Materials 5 (2022) 486–514. https://doi.org/10.1002/eem2.12237.

[60] S.M. Nakhmanson, M.B. Nardelli, J. Bernholc, Collective polarization effects in β - polyvinylidene fluoride and its copolymers with tri- and tetrafluoroethylene, Phys. Rev. B 72 (2005) 115210. https://doi.org/10.1103/PhysRevB.72.115210.

[61] R. Gregorio, E.M. Ueno, Effect of crystalline phase, orientation and temperature on the dielectric properties of poly (vinylidene fluoride) (PVDF), Journal of Materials Science 34 (1999) 4489–4500. https://doi.org/10.1023/A:1004689205706.

[62] L. Yang, J. Ho, E. Allahyarov, R. Mu, L. Zhu, Semicrystalline Structure–Dielectric Property Relationship and Electrical Conduction in a Biaxially Oriented Poly(vinylidene fluoride) Film under High Electric Fields and High Temperatures, ACS Appl. Mater. Interfaces 7 (2015) 19894–19905. https://doi.org/10.1021/acsami.5b02944.

[63] T. Wu, H. Jin, S. Dong, W. Xuan, H. Xu, L. Lu, Z. Fang, S. Huang, X. Tao, L. Shi, S. Liu, J. Luo, A Flexible Film Bulk Acoustic Resonator Based on β-Phase Polyvinylidene Fluoride Polymer, Sensors 20 (2020) 1346. https://doi.org/10.3390/s20051346.

[64] A. Morali, A. Mandal, M. Skorobogatiy, S. Bodkhe, Unleashing the piezoelectric potential of PVDF: a study on phase transformation from gamma (γ) to beta (β) phase through thermal contact poling, RSC Adv. 13 (2023) 31234–31242. https://doi.org/10.1039/D3RA05068H.

[65] J.Y. Lim, S. Kim, Y. Seo, Enhancement of β-phase in PVDF by electrospinning, in: Cleveland, Ohio, USA, 2015: p. 070006. https://doi.org/10.1063/1.4918441.

[66] N. Soin, D. Boyer, K. Prashanthi, S. Sharma, A.A. Narasimulu, J. Luo, T.H. Shah, E. Siores, T. Thundat, Exclusive self-aligned β-phase PVDF films with abnormal piezoelectric coefficient prepared via phase inversion, Chem. Commun. 51 (2015) 8257–8260. https://doi.org/10.1039/C5CC01688F.

[67] H.H. Singh, S. Singh, N. Khare, Enhanced β -phase in PVDF polymer nanocomposite and its application for nanogenerator, Polymers for Advanced Techs 29 (2018) 143–150. https://doi.org/10.1002/pat.4096.

[68] Md.N. Islam, R.H. Rupom, P.R. Adhikari, Z. Demchuk, I. Popov, A.P. Sokolov, H.F. Wu, R.C. Advincula, N. Dahotre, Y. Jiang, W. Choi, Boosting Piezoelectricity by 3D Printing PVDF-MoS_2 Composite as a Conformal and High-Sensitivity Piezoelectric Sensor, Adv Funct Materials 33 (2023) 2302946. https://doi.org/10.1002/adfm.202302946.

[69] R.H. Rupom, M.N. Islam, Z. Demchuk, R. Advincula, N.B. Dahotre, Y. Jiang, W. Choi, Tailoring Piezoelectricity of 3D Printing PVDF-MoS_2 Nanocomposite via In Situ Induced Shear Stress, ACS Appl. Nano Mater. 7 (2024) 22714–22722. https://doi.org/10.1021/acsanm.4c03695.

[70] P. Han, A. Tofangchi, D. Carr, S. Zhang, K. Hsu, Enhancing the Piezoelectric Properties of 3D Printed PVDF Using Concurrent Torsional Shear Strain, Polymers 15 (2023) 4204. https://doi.org/10.3390/polym15214204.

[71] X. Yuan, A. Yan, Z. Lai, Z. Liu, Z. Yu, Z. Li, Y. Cao, S. Dong, A poling-free PVDF nanocomposite via mechanically directional stress field for self-powered pressure sensor application, Nano Energy 98 (2022) 107340. https://doi.org/10.1016/j.nanoen.2022.107340.

[72] G.-J. Choi, S.-H. Sohn, S.-J. Kim, I.-K. Park, Polymer Composite-Based Triboelectric Nanogenerators: Recent Progress, Design Principles, and Future Perspectives, Polymers 17 (2025) 1962. https://doi.org/10.3390/polym17141962.

[73] K.K. Meena, I. Arief, A. Nag, J. Nagel, A. Das, 3D-Printed PVDF-Based Hybrid Nanogenerators With Dominant Triboelectric Output for High-Sensitivity Force Sensing, IEEE Sensors J. 25 (2025) 26412–26420. https://doi.org/10.1109/JSEN.2025.3572337.

[74] M.A. Kashfipour, N. Mehra, J. Zhu, A review on the role of interface in mechanical, thermal, and electrical properties of polymer composites, Adv Compos Hybrid Mater 1 (2018) 415–439. https://doi.org/10.1007/s42114-018-0022-9.

[75] Y. Li, X. Huang, L. Zeng, R. Li, H. Tian, X. Fu, Y. Wang, W.-H. Zhong, A review of the electrical and mechanical properties of carbon nanofiller-reinforced polymer composites, J Mater Sci 54 (2019) 1036–1076. https://doi.org/10.1007/s10853-018-3006-9.

[76] P.M. Ajayan, L.S. Schadler, P.V. Braun, eds., Nanocomposite Science and Technology, 1st ed., Wiley, 2003. https://doi.org/10.1002/3527602127.

[77] Md.N. Islam, Z. Smith, R.H. Rupom, R. Rijal, Z. Demchuk, N. Dahotre, H.F. Wu, R.C. Advincula, W. Choi, Y. Jiang, Self-Sensing Composites via an Embedded 3D-Printed PVDF-MoS_2 Nanosensor for Structural Health Monitoring, ACS Appl. Mater. Interfaces 17 (2025) 36026–36033. https://doi.org/10.1021/acsami.5c05683.

[78] M.-J. Wang, Effect of Polymer-Filler and Filler-Filler Interactions on Dynamic Properties of Filled Vulcanizates, Rubber Chemistry and Technology 71 (1998) 520–589. https://doi.org/10.5254/1.3538492.

[79] N. Ichinose, M. Ishikawa, K. Morimoto, Effect of stress transfer between fiber and matrix on toughness of polymer composite, Polymer Composites 32 (2011) 1617–1624. https://doi.org/10.1002/pc.21200.

[80] M.C. Araújo, C.M. Costa, S. Lanceros-Méndez, Evaluation of dielectric models for ceramic/polymer composites: Effect of filler size and concentration, Journal of Non-Crystalline Solids 387 (2014) 6–15. https://doi.org/10.1016/j.jnoncrysol.2013.12.005.

[81] S.-Y. Fu, X.-Q. Feng, B. Lauke, Y.-W. Mai, Effects of particle size, particle/matrix interface adhesion and particle loading on mechanical properties of particulate–polymer composites,

Composites Part B: Engineering 39 (2008) 933–961. https://doi.org/10.1016/j.compositesb.2008.01.002.

[82] W. Bauhofer, J.Z. Kovacs, A review and analysis of electrical percolation in carbon nanotube polymer composites, Composites Science and Technology 69 (2009) 1486–1498. https://doi.org/10.1016/j.compscitech.2008.06.018.

[83] J.C.H. Affdl, J.L. Kardos, The Halpin-Tsai equations: A review, Polymer Engineering & Sci 16 (1976) 344–352. https://doi.org/10.1002/pen.760160512.

[84] H. Huang, J. Zhang, Effects of filler–filler and polymer–filler interactions on rheological and mechanical properties of HDPE–wood composites, J of Applied Polymer Sci 111 (2009) 2806–2812. https://doi.org/10.1002/app.29336.

[85] K.S. Ramadan, D. Sameoto, S. Evoy, A review of piezoelectric polymers as functional materials for electromechanical transducers, Smart Mater. Struct. 23 (2014) 033001. https://doi.org/10.1088/0964-1726/23/3/033001.

[86] A. Katheria, J. Nayak, N.Ch. Das, A journey of thermoplastic elastomer nanocomposites for electromagnetic shielding applications: from bench to transitional research, Mater. Adv. 3 (2022) 2670–2691. https://doi.org/10.1039/D1MA00989C.

[87] A. Bouhamed, N. Jöhrmann, S. Naifar, B. Böhm, O. Hellwig, B. Wunderle, O. Kanoun, Collaborative Filler Network for Enhancing the Performance of BaTiO3/PDMS Flexible Piezoelectric Polymer Composite Nanogenerators, Sensors 22 (2022) 4181. https://doi.org/10.3390/s22114181.

[88] H.-J. Choi, M.S. Kim, D. Ahn, S.Y. Yeo, S. Lee, Electrical percolation threshold of carbon black in a polymer matrix and its application to antistatic fibre, Sci Rep 9 (2019) 6338. https://doi.org/10.1038/s41598-019-42495-1.

[89] E.T. Thostenson, Z. Ren, T.-W. Chou, Advances in the science and technology of carbon nanotubes and their composites: a review, Composites Science and Technology 61 (2001) 1899–1912. https://doi.org/10.1016/S0266-3538(01)00094-X.

[90] Z.-M. Dang, J.-K. Yuan, J.-W. Zha, T. Zhou, S.-T. Li, G.-H. Hu, Fundamentals, processes and applications of high-permittivity polymer–matrix composites, Progress in Materials Science 57 (2012) 660–723. https://doi.org/10.1016/j.pmatsci.2011.08.001.

[91] Y. Zare, K.Y. Rhee, Model Progress for Tensile Power of Polymer Nanocomposites Reinforced with Carbon Nanotubes by Percolating Interphase Zone and Network Aspects, Polymers 12 (2020) 1047. https://doi.org/10.3390/polym12051047.

[92] M. Bhong, T.K.H. Khan, K. Devade, B. Vijay Krishna, S. Sura, H.K. Eftikhaar, H. Pal Thethi, N. Gupta, Review of composite materials and applications, Materials Today: Proceedings (2023) S2214785323049313. https://doi.org/10.1016/j.matpr.2023.10.026.

[93] X. Zhang, P. Wang, Y. Zhou, X. Li, E.-H. Yang, T.X. Yu, J. Yang, The effect of strain rate and filler volume fraction on the mechanical properties of hollow glass microsphere modified polymer, Composites Part B: Engineering 101 (2016) 53–63. https://doi.org/10.1016/j.compositesb.2016.06.079.

[94] A.S. Doumbia, A. Bourmaud, D. Jouannet, T. Falher, F. Orange, R. Retoux, L. Le Pluart, L. Cauret, Hollow microspheres – poly-(propylene) blends: Relationship between microspheres degradation and composite properties, Polymer Degradation and Stability 114 (2015) 146–153. https://doi.org/10.1016/j.polymdegradstab.2014.12.024.

[95] G. Tagliavia, M. Porfiri, N. Gupta, Analysis of flexural properties of hollow-particle filled composites, Composites Part B: Engineering 41 (2010) 86–93. https://doi.org/10.1016/j.compositesb.2009.03.004.

[96] N. Gupta, S.E. Zeltmann, V.C. Shunmugasamy, D. Pinisetty, Applications of Polymer Matrix Syntactic Foams, JOM 66 (2014) 245–254. https://doi.org/10.1007/s11837-013-0796-8.

[97] S. Ferdousi, R. Advincula, A.P. Sokolov, W. Choi, Y. Jiang, Investigation of 3D printed lightweight hybrid composites via theoretical modeling and machine learning, Composites Part B: Engineering 265 (2023) 110958. https://doi.org/10.1016/j.compositesb.2023.110958.

[98] O.A. Afolabi, M.T. Pandurangan, K. Kanny, Effect of Hollow Glass Microsphere (HGM) on Impact and Flexural Properties of High-Density Syntactic Foam Based Epoxy Composites, Materials Today: Proceedings 87 (2023) 246–251. https://doi.org/10.1016/j.matpr.2023.05.351.

[99] A. Mondal, M.C. Saha, Y. Jiang, D. Rhule, J.E.C. Sabisch, Direct ink writing of hexagonal honeycomb carbon fiber-reinforced epoxy composites with varying cell geometric parameters and tailored in-plane compressive properties, Polymer Composites 46 (2025). https://doi.org/10.1002/pc.29767.

[100] Y. Jiang, L.M. Korpas, J.R. Raney, Bifurcation-based embodied logic and autonomous actuation, Nat Commun 10 (2019) 128. https://doi.org/10.1038/s41467-018-08055-3.

[101] D.A. Rau, C.B. Williams, M.J. Bortner, Rheology and printability: A survey of critical relationships for direct ink write materials design, Progress in Materials Science 140 (2023) 101188. https://doi.org/10.1016/j.pmatsci.2023.101188.

[102] S. Jiang, Q. Cai, Y. Jiang, R.Z. Gan, Effect of liraglutide treatment on mitigation of hearing damage induced by multiday repeated high-intensity blasts, The Journal of the Acoustical Society of America 158 (2025) 1431–1442. https://doi.org/10.1121/10.0039047.

[103] S. Jiang, P. Welch, S. Sanders, R.Z. Gan, Mitigation of Hearing Damage After Repeated Blast Exposures in Animal Model of Chinchilla, JARO 23 (2022) 603–616. https://doi.org/10.1007/s10162-022-00862-2.

[104] K.Y. Patiño Jaimes, E.B. Caldona, E.M. Kim, J. Lambert, E.C. Winn, E.L. Ribeiro, Y. Jiang, S. Ferdousi, B. Hicks, Y. Wang, I.N. Ivanov, R.C. Advincula, Distinct Mechanism of Anti-Corrosion and Swelling-Adhesion Modeling of Low-Dimensional Nylon-Fluoropolymer Composite Coatings, ACS Appl. Polym. Mater. 6 (2024) 3049–3059. https://doi.org/10.1021/acsapm.3c02335.

[105] P.C. Hiemenz, T.P. Lodge, Polymer chemistry, 2nd ed, CRC Press, Boca Raton, 2007.

[106] M.L. Williams, R.F. Landel, J.D. Ferry, The Temperature Dependence of Relaxation Mechanisms in Amorphous Polymers and Other Glass-forming Liquids, J. Am. Chem. Soc. 77 (1955) 3701–3707. https://doi.org/10.1021/ja01619a008.

[107] K.L. Ngai, Relaxation and Diffusion in Complex Systems, Springer New York, New York, NY, 2011. http://link.springer.com/10.1007/978-1-4419-7649-9 (accessed January 20, 2026).

[108] Y. Hu, R. Mei, Z. An, J. Zhang, Silicon rubber/hollow glass microsphere composites: Influence of broken hollow glass microsphere on mechanical and thermal insulation property, Composites Science and Technology 79 (2013) 64–69. https://doi.org/10.1016/j.compscitech.2013.02.015.

[109] W.N. Dos Santos, C.Y. Iguchi, R. Gregorio, Thermal properties of poly(vinilidene fluoride) in the temperature range from 25 to 210 °C, Polymer Testing 27 (2008) 204–208. https://doi.org/10.1016/j.polymertesting.2007.10.005.

[110] N. Chandra, S. Ganpule, N.N. Kleinschmit, R. Feng, A.D. Holmberg, A. Sundaramurthy, V. Selvan, A. Alai, Evolution of blast wave profiles in simulated air blasts: experiment and computational modeling, Shock Waves 22 (2012) 403–415. https://doi.org/10.1007/s00193-012-0399-2.